



**HAL**  
open science

# Can Paints and Varnish Impair the Physicochemical Properties of Wood Pyrolysis Oils?

W. Locatel, D. Laurenti, Y. Schuurman, N. Guilhaume

► **To cite this version:**

W. Locatel, D. Laurenti, Y. Schuurman, N. Guilhaume. Can Paints and Varnish Impair the Physicochemical Properties of Wood Pyrolysis Oils?. *Energy & Fuels*, 2021, 35 (21), pp.17739-17754. 10.1021/acs.energyfuels.1c02568 . hal-03438859

**HAL Id: hal-03438859**

**<https://hal.science/hal-03438859>**

Submitted on 18 Aug 2022

**HAL** is a multi-disciplinary open access archive for the deposit and dissemination of scientific research documents, whether they are published or not. The documents may come from teaching and research institutions in France or abroad, or from public or private research centers.

L'archive ouverte pluridisciplinaire **HAL**, est destinée au dépôt et à la diffusion de documents scientifiques de niveau recherche, publiés ou non, émanant des établissements d'enseignement et de recherche français ou étrangers, des laboratoires publics ou privés.

1 **Can paints and varnish impair the physicochemical properties of wood pyrolysis oils ?**

2 William de Rezende Locatel, Dorothée Laurenti, Yves Schuurman, Nolven Guillaume\*

3 Univ. Lyon, Université Claude Bernard Lyon 1, CNRS, IRCELYON – UMR 5256, 2 Avenue  
4 Albert Einstein, F-69626 Villeurbanne Cedex, France

5  
6 \* Corresponding author, [nolven.guilhaume@ircelyon.univ-lyon1.fr](mailto:nolven.guilhaume@ircelyon.univ-lyon1.fr)

7 Abstract

8 The use of pyrolysis oils from demolition woods is an interesting option to produce fuels or  
9 chemicals from waste wood. This work investigated the effect of paints and varnish, that contain  
10 various potential contaminants, on the properties of bio-oils obtained by thermal pyrolysis of wood  
11 or after *ex-situ* catalysis of the pyrolysis vapors using a H-ZSM-5 catalyst. The paints and varnish  
12 were analyzed and their main inorganic components identified. Clean beech wood samples were  
13 impregnated with commercial paints and varnish, and also individually with the main inorganic  
14 compounds (TiO<sub>2</sub>, CaCO<sub>3</sub>, BaSO<sub>4</sub>) found in the paints and varnish. These contaminated wood  
15 samples were pyrolyzed and the gas, liquid and solid products formed were thoroughly  
16 characterized, and compared to the products obtained from clean wood. The results show that the  
17 mineral contaminants remained in the chars and that the pyrolysis oils obtained by thermal  
18 pyrolysis were not significantly modified by the presence of contaminants on the wood. In *ex-situ*  
19 catalyzed pyrolysis experiments, the H-ZSM-5 catalyst promoted the formation of some fully  
20 deoxygenated aromatic compounds, which were not obtained without catalyst. However, the bio-  
21 oil produced from wood impregnated with commercial paints and varnish contained less fully  
22 deoxygenated compounds. This effect was not related to the mineral compounds present in the  
23 paints and varnish and could originate from the polymeric organic components present in their  
24 formulations.

25 The Waste2Road project has received funding from the European Union's Horizon 2020 research  
26 and innovation programme under grant agreement N° 818120.

27  
28 Keywords:

29 Wood pyrolysis; Demolition wood; Paints and varnish; Ex-situ catalytic upgrading; H-ZSM-5.

## 30 1 INTRODUCTION

31 Co-processing pyrolysis-oils with fossil oils in conventional refining facilities, such as  
32 fluid catalytic cracking (FCC) or hydrodeoxygenation (HDO) units, can contribute to reduce fossil  
33 fuels dependency without heavy investments. However, the percentage of bio-oils that can be  
34 mixed with fossil oils is limited, due to their detrimental impact on catalysts. For example, Pinho  
35 et al. <sup>1</sup> showed that up to 10 wt.% of pyrolysis oil can be processed with Brazilian vacuum gasoil  
36 (VGO) in a FCC demonstration-scale unit (150 kg/h) without significant impact on products yields  
37 and quality. The option of using biogenic residues and waste biomass is even more attractive to  
38 develop a new generation of cost-effective biofuels and to improve waste management and  
39 recycling. For instance, construction and demolition materials represent around 32% of the total  
40 waste streams in the European Union (EU), accounting for more than 800 millions tons per year <sup>2</sup>.  
41 Aiming to mitigate this issue, the EU adopted in 2008 the Waste Framework Directive <sup>3</sup>, setting a  
42 minimum target of 70 wt.% recovery, recycling and re-use by 2025 for construction and demolition  
43 waste (CDW). CDW is composed at  $\approx$ 85% concrete, ceramics and masonry materials, while  
44 woody materials represents 2 - 4% <sup>4</sup>, which represents substantial tonnages due to the large  
45 amounts of waste produced. Therefore, pyrolysis of demolition wood could be an alternative to re-  
46 use this organic fraction of CDW, given that this process has been proved suitable for many  
47 different types of biomass <sup>5</sup>.

48 Numerous studies investigated the effect of different parameters of pyrolysis, such as  
49 temperature, heating rate, particle size, reactor configuration, residence time, presence and  
50 properties of catalyst (<sup>6, 7, 8, 9, 10, 11, 12</sup>); other works reported the impact of mixing the wood with  
51 different materials such as plastics, agricultural residues and municipal solid waste (<sup>13, 14, 15, 16</sup>).  
52 The pyrolysis of demolition wood in a fluidized bed reactor has been mentioned as early as 2005<sup>17</sup>,  
53 but the authors reported mostly experiments using pristine woods (pine, beech, bamboo) and only  
54 one using demolition wood, which were simply compared in terms of liquids and chars yields.  
55 Hwang et al. <sup>18</sup> carried out the pyrolysis of different municipal solid wastes including wood chips  
56 (obtained from construction and demolition waste) and mixtures of paper/wood/plastics, at 500,  
57 700 and 900°C, the highest temperatures more closely related to gasification conditions. The gas  
58 production increased with temperature at the expense of liquid products, which were quantified  
59 but lacked detailed characterizations.

60 Compared to pristine wood, demolition wood contains various pollutants originating from  
61 the products applied for wood preservation, decoration and protection: persistent organic  
62 pollutants (POPs) from wood preservatives, metal oxides and organic compounds from paints,  
63 varnishes and flame retardancy treatments.

64 The composition of modern waterborne paints is complex: in addition to the purely mineral  
65 pigments (Ti, Cr, Zn, Fe, Cd, Co oxides) or metal-organic pigments (i.e. “phthalo blue” based on  
66 copper phthalocyanin, “nickel azo yellow” based on azonium complexes) that give the colors, they  
67 also contain binders (water-dispersible acrylic or vinylic based copolymers of high molecular mass  
68 that form a continuous film on the substrate surface) and several additives such as plasticizers (i.e.  
69 dimethylphthalate), defoamers (i.e. silicon oil), stabilizers (i.e. dimethylformamide,  
70 dibutyldithiocarbamate), metal soaps (i.e. Al stearate), dispersing agents (i.e. polyphosphates) and  
71 extenders or fillers (i.e. CaCO<sub>3</sub>, BaSO<sub>4</sub>, talc, mica) used to improve the paints properties  
72 (durability, viscosity, film adhesion and hardness, corrosion resistance) and to decrease their cost  
73 <sup>19, 20</sup>. Their effect on the properties and quality of pyrolysis oils prepared from waste wood has  
74 been scarcely studied. Özbay et al. <sup>21</sup> studied the effect of three different varnishes deposited on  
75 pine wood on the properties of the derived pyrolysis oils. Although the main components of bio-  
76 oils identified by GC-MS were not drastically different in the oils derived from pure wood or wood  
77 impregnated with varnishes, their yields were different in the presence of varnishes, the  
78 polyurethane varnish leading to a higher yield in phenols, and the chemical composition of the oils  
79 was significantly modified. More specifically, the effect of metal catalysts in biomass fast  
80 pyrolysis has been studied by two approaches: either by direct impregnation of catalysts on the  
81 biomass, or by ex-situ catalysis, in which the vapors produced by thermal pyrolysis pass through  
82 a bed of catalyst. In the first case, the biomass is generally impregnated to the core by using  
83 solutions of metal salts. Inorganic compounds such as CaCO<sub>3</sub> and BaSO<sub>4</sub> have been shown to  
84 interact with biomass through a mineralization process and to modify its structural properties <sup>22, 23,</sup>  
85 <sup>24, 25</sup> and consequently the pyrolysis process and the composition of bio-oils derived from it. As  
86 regards ex-situ catalysis, many metal oxides, including TiO<sub>2</sub>, have been reported to exhibit a  
87 catalytic activity to upgrade pyrolysis vapors <sup>26, 27</sup> but H-ZSM-5 is the most widely used catalyst  
88 to promote bio-oils deoxygenation in absence of hydrogen by dehydroxylation, decarboxylation  
89 or decarbonylation reactions.

90           Considering that the organic components of paints can degrade at the pyrolysis  
91 temperature, while their mineral components can modify the thermal processes leading to the  
92 formation of pyrolysis oils, the objective of the present study was to assess the impact of paints  
93 and varnish on the properties of bio-oils obtained by fast pyrolysis of beech wood. This effect was  
94 compared in purely thermal pyrolysis experiments and in the presence of an H-ZSM-5 catalyst for  
95 ex-situ catalytic treatment of the pyrolysis vapors. In this purpose, model contaminated woods  
96 were prepared by impregnation of beech wood chips with three commercial paints of different  
97 colors (because they contain different inorganic pigments) and one varnish, and pyrolyzed in  
98 purely thermal or thermal + catalyzed experiments. The effect of paints and varnish was evaluated  
99 by quantifying the gas, liquid and solid products obtained by pyrolysis of clean and impregnated  
100 woods and by comparing their physicochemical properties using various characterization  
101 techniques. In addition, the main mineral compounds present in the paints and varnish were  
102 identified and individually deposited on the pristine wood chips to ascribe more specifically which  
103 of them might modify the reactions involved in the pyrolysis process, or behave as catalysts to  
104 promote reactions between components of the pyrolysis vapors.

## 105 2 EXPERIMENTAL SECTION

106

### 107 2.1 Clean and contaminated woods.

108           Clean wood samples were prepared from commercial beech wood chips supplied by J.  
109 Rettenmaier & Söhne (JRS) and sieved to a particle size range between 0.75 and 1.7 mm. The bulk  
110 density was obtained by measuring the mass of sample representing the volume of 100 mL. The  
111 elemental composition (CHNS) was obtained with a Flash2000 (Thermo Scientific) equipment.

112           The compounds hereafter referred to as “contaminants” were four different commercial  
113 products: one varnish (Mat profond/Chêne clair – V33) and three acrylic-based paints of different  
114 colors (White: Velours/North pole – Good home/Castorama; Yellow: Premium/Argan – Tollens;  
115 Blue: Bleu gris – Dulux Valentine). The volatile matter of contaminants was determined by drying  
116 a weighed sample at room temperature for 48h, then at 90°C for 24h, and weighing the mass  
117 remaining after this process. The contaminated woods were prepared using an aqueous suspension  
118 of varnish and paints (in equal mass proportion), aiming to obtain a final mass of 5 wt. % of  
119 pollutants (on dry basis). The wood chips were added to this suspension (water/biomass ratio: 3.75  
120 mL/g) and the mixture was stirred in a rotary evaporator at room temperature and atmospheric

121 pressure for 1h. Then the water was evaporated by heating the bath at 50°C under reduced pressure  
122 (400 mbar). The wood chips were dried in air at room temperature for 3 days, divided in small  
123 fractions with the exact mass of wood needed for each experiment and kept in tightly closed vials.  
124 Additionally, all wood samples were dried in an oven at 110°C before pyrolysis experiments.

125 The ash content of paints and varnish was obtained after calcination in air at 600°C for 3 h  
126 and characterized by X-ray fluorescence (XRF) using a Panalytical Epsilon 4 spectrometer.  
127 Samples were analyzed as powders deposited in plastic cups covered with Mylar film. The  
128 elements were identified using a semi-quantitative method (Omnian), which allows quantification  
129 of elements in the ppm range. The crystalline phases were identified by X-ray diffraction (XRD)  
130 using a Bruker D8 Advanced A25 diffractometer, with 2 $\theta$  range from 4° to 80° and steps of 0.02°.  
131 The diffractograms were analyzed using the Diffract Eva software associated with the PDF4+  
132 database (2021).

133 ATR-FTIR spectra of pure PMMA, dry paints and varnish were recorded in the 4000-650  
134 cm<sup>-1</sup> range at a resolution of 4 cm<sup>-1</sup> with accumulation of 128 scans, using a Cary 630 FTIR  
135 spectrometer (Agilent Technologies) equipped with an ATR sampling module (diamond crystal  
136 and ZnSe windows).

137 The thermal decomposition of the wood was studied by thermogravimetric analysis (TGA),  
138 under N<sub>2</sub> or air (40 mL/min) between 25°C and 900 °C (heating rate 10°C/min) on a Setsys  
139 Evolution 1200 (SETARAM) analyzer with approximately 10 mg of initial mass.

## 140 **2.2 Catalyst.**

141

142 An H-ZSM-5 catalyst with a Si/Al ratio of 40 was supplied by Céramiques Techniques  
143 Industrielles (CTI) Salindres, France. The powder was sieved to a particle size between 100 and  
144 300  $\mu\text{m}$ . The textural properties of catalysts were characterized by nitrogen adsorption at -196 °C  
145 on a Belsorp II adsorption measurements apparatus, after desorption at 200 °C under vacuum for  
146 14 h. The specific surface area and total pore volume were calculated using the Brunauer-Emmett-  
147 Teller (BET) equation and the Barrett-Joyner-Teller (BJH) method was applied to calculate the  
148 average pore diameter. Its main properties are summarized in Table 1.

149

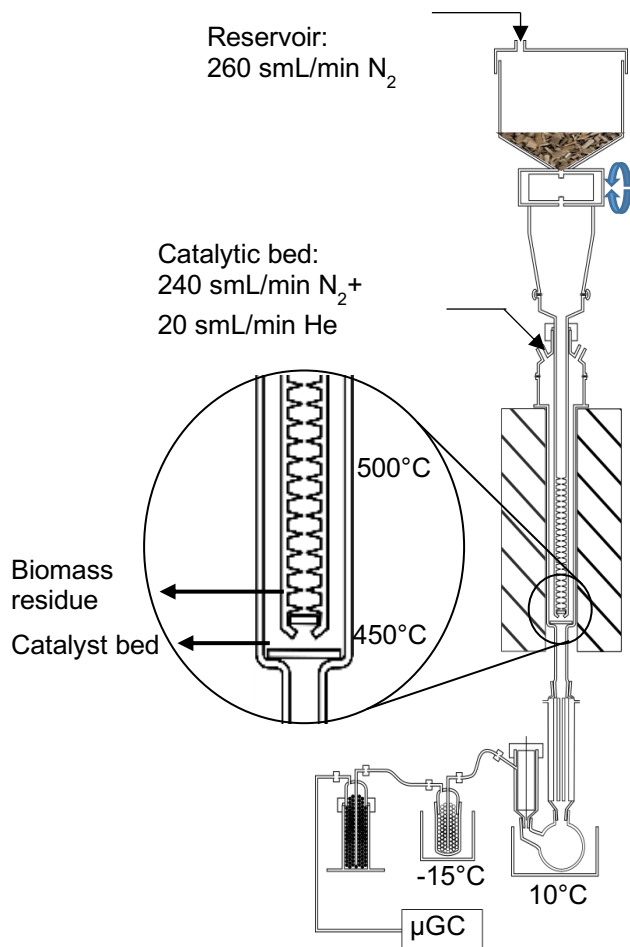
150 Table 1 – Properties of H-ZSM-5 catalyst

Property	Value
Si/Al atomic ratio (SAR)	40.5
Total SSA <sup>a</sup> (m <sup>2</sup> g <sup>-1</sup> )	423
microporous surface (m <sup>2</sup> g <sup>-1</sup> )	363
external surface (m <sup>2</sup> g <sup>-1</sup> )	60
Average pore diameter <sup>b</sup> (nm)	0.55
Total pore volume (cm <sup>3</sup> g <sup>-1</sup> )	0.18
Brønsted acid sites (μmol/g) <sup>c</sup>	127
Lewis acid sites (μmol/g) <sup>c</sup>	45

151 <sup>a</sup> BET method; <sup>b</sup> from International Zeolite Association database; <sup>c</sup> measured by FT-IR of pyridine  
 152 adsorbed at 150°C.

### 153 2.3 Pyrolysis set-up and products recovery procedure.

154 A lab-scale pyrolytic set-up already described previously <sup>10</sup> was used. The wood chips were  
 155 dried at 110°C for 1.5 h before being placed in a gas-tight hopper and kept under N<sub>2</sub>. A solid  
 156 dispenser allowed the semi-continuous delivery of the wood chips (every 10 seconds), with a  
 157 feeding rate of ≈16 g/h. The wood chips fall by gravity in a quartz tubular reactor equipped with  
 158 internal spikes to slow down the fall and increase the residence time of wood particles in the  
 159 pyrolysis section (Figure 1). At the bottom of the pyrolysis zone, a first quartz frit collects the solid  
 160 residues, while the vapors are driven through the catalytic bed placed downstream on a second frit.  
 161 The reactor is heated by a tubular oven which regulated the pyrolysis section temperature to 500°C  
 162 and the catalyst temperature to 450°C. Two inert gas flows are dispensed separately in the two  
 163 reactor parts: 260 smL/min of N<sub>2</sub> from the wood hopper to the pyrolysis section (this flow serves  
 164 to keep the wood chips under inert atmosphere and to drive the pyrolysis vapors towards the  
 165 catalyst bed) and 240 smL/min of N<sub>2</sub> + 20 smL/min of He (internal standard) are sent directly to  
 166 the catalytic bed (this flow is used to prevent retro-diffusion of vapors and to adjust the total gas  
 167 flow rate).



168

169 Figure 1 - Pyrolysis set-up scheme

170 A trap system including A) a condenser and a round bottom flask at 10°C, B) an electrostatic  
 171 precipitator, C) a trap filled with Pyrex beads at -15°C and D) a silica gel beads trap at ambient  
 172 temperature, prevents any condensable liquids from reaching the on-line micro-GC analyzer. The  
 173 total mass of bio-oils formed in the experiments was established by mass difference, by weighing  
 174 the different glassware parts before and after the experiments. The first fraction of bio-oil was  
 175 recovered after condensation in the first cold trap at 10°C and hereafter denoted as the “organic  
 176 phase”. Due to its direct recovery in the first cold trap, this phase was considered the most  
 177 representative of the native bio-oil composition. Other portions were also recovered downstream  
 178 in the different parts of the glassware assembly (cold traps, electrostatic precipitator) and hereafter  
 179 denoted as “recovered organic phase”. The recovery process involved washing the different  
 180 glassware parts with methanol, gathering the washing fractions and evaporating the methanol,  
 181 which probably involved the simultaneous evaporation of volatile bio-oils components. Therefore,

182 the “recovered organic phase” was quantified and characterized separately. Indeed, Karl-Fischer  
183 titration of the recovered fractions revealed that they contained less water than the pristine organic  
184 phase, whereas <sup>13</sup>C-NMR analyses showed that they contained residual methanol. Therefore, since  
185 the recovery process appeared to modify the bio-oil composition, it was decided not to mix these  
186 fractions. Finally, the “unrecovered organic phase” was deposited on the Pyrex beads and in the  
187 silicagel beads trap; this fraction was only weighed for total bio-oil quantification, because its  
188 recovery would have involved too much solvent or because it was not possible to extract it from  
189 the silicagel.

190 The mass of solid residue deposited on the first frit glass was weighed, whereas the  
191 incondensable gaseous products were quantified by GC and converted to a mass of gaseous  
192 products, in order to determine the mass balance of gas, liquid and solid products. In catalytic  
193 experiments, 2 g of catalyst were used (discounting the water content determined by TGA). Before  
194 starting the wood delivery, the reactor was heated to 500 °C under N<sub>2</sub> for 1 h in order to reach a  
195 stable temperature and to desorb the catalyst in *ex-situ* catalytic pyrolysis experiments.

196

#### 197 **2.4 Products analysis.**

198 The gaseous products were analyzed on-line during the pyrolysis experiments using a  
199 micro gas chromatograph Inficon 3000 (SRA instruments) equipped with three analytical modules  
200 (MolSieve, Plot U and Alumina columns) to identify and quantify all the gaseous compounds  
201 produced (He, H<sub>2</sub>, CO, CO<sub>2</sub> and C<sub>1</sub>-C<sub>5</sub> hydrocarbons). Each analysis duration was 6 minutes and  
202 they were run successively for 90 minutes. The GC response of all gaseous compounds was  
203 calibrated using appropriate calibration mixtures. Helium was used as internal standard for  
204 quantitative analysis, because the production of gaseous compounds resulted in a reactor exit gas  
205 stream higher than the inlet gas flow rate.

206 The water content of bio-oils was determined by Karl-Fischer Titration, using a Metrohm  
207 Titrand 852 analyzer. The samples were diluted in THF (≈ 10 %wt.) and the volumetric method  
208 was employed. To avoid possible side reactions of aldehydes and ketones with standard reagents,  
209 which produce water and alter the water quantification, the reagents were specifically chosen for  
210 samples containing these organic compounds: Karl Fischer ROTI hydroquant C5K (5 mg of

211 water/mL of solution) and Karl Fischer ROTI hydroquant working medium K. The calibration was  
212 carried out using Hydranal – Water Standard 10.0.

213 Total organic carbon (TOC) measurements were performed with a Shimadzu TOC-VCHS  
214 analyzer equipped with an ASI-V sampler. Samples were diluted in ultrapure water (0.1 wt.%) and  
215 mixed with hydrochloric acid (concentration 1N) to remove the inorganic carbon as CO<sub>2</sub>. Then,  
216 the samples were injected in a combustion reactor with a catalytic bed of Pt/Al<sub>2</sub>O<sub>3</sub> at 720 °C. The  
217 gas phase was cooled down and dried and the CO<sub>2</sub> produced was analyzed by an IR detector.  
218 External calibration was applied, using a solution of nicotinic acid (0.1 g/L). Two measurements  
219 were generally carried out, three if the standard deviation between the first two measurements was  
220 greater than 2%.

221 The average molar mass and molar mass distributions were obtained by gel permeation  
222 chromatography (GPC). The measurements were performed with an Agilent equipment (1200  
223 series) using two PL gel columns with different pore sizes (500 and 50 Å) equipped with a  
224 refractive index detector (RID) and a diode-array detector (DAD), collecting spectra every 0.4 s  
225 in the range 200-450 nm, each 2 nm. The mobile phase used was THF with flow rate of 1 mL/min.  
226 The samples were dissolved in THF with a concentration of 0.2 wt. % for the organic fraction and  
227 1 wt. % for the aqueous phase, and filtered before analysis. The measurements were carried out at  
228 35°C and the system was calibrated using hydrocarbons (HC) standards of molecular weights  
229 between 86 and 1000 g/mol. The calibration with HCs showed a smaller deviation regarding the  
230 real molar mass of reference compounds than the traditional PS calibration. The reference  
231 compounds were eugenol (164 g/mol) and 1-(2,4-Dihydroxyphenyl)-2-(4-methoxyphenoxy)  
232 ethenone (274 g/mol), denoted as DHPMPE. The difference between measured and real MWs was  
233 <-15 % with HC calibration, but up to +70% with PS calibration. When the UV detector was used,  
234 the signal was normalized per mass unit of dry bio-oil, this correction being possible because the  
235 absorption of pure water in this wavelength range is very weak and can be neglected.

236 <sup>13</sup>C-NMR spectra were recorded with a spectrometer Bruker AVANCE 400 MHz and the  
237 spectra were analyzed using TopSpin 3.0 software. The measurements were performed at room  
238 temperature with accumulation of 4500 scans. The samples were placed in the tube and a thinner  
239 tube containing DMSO-D<sub>6</sub> was inserted, allowing to recover the oil-samples without modification  
240 after the analysis. Trioxane was used as an internal standard, diluted in DMSO-D<sub>6</sub> to allow the

241 quantification of functional groups. The choice of trioxane is due to its specific chemical shift (at  
242 93 ppm) that is well defined and does not overlap with other peaks of the bio-oils.

243 Gas chromatograph coupled with a mass spectrometer (Shimadzu GCMS-QP2010 SE)  
244 equipped with a Zebron ZB Wax-Plus column (60 m, 0.25 mm I.D., film thickness 0.25  $\mu\text{m}$ ) was  
245 employed to analyze the organic fractions diluted in methanol (20 wt. %). The aqueous phases  
246 were diluted in methanol at a concentration of 30 wt. %. The oven temperature program starts at  
247 70  $^{\circ}\text{C}$  (hold for 10 min), then heating rate of 5 $^{\circ}\text{C}/\text{min}$  up to 150  $^{\circ}\text{C}$ . At this point the heating rate  
248 changes to 3 $^{\circ}\text{C}/\text{min}$  up to 250  $^{\circ}\text{C}$  (hold for 15 min).

249 The two-dimensional gas chromatography coupled with mass spectrometry (GCxGC-MS)  
250 was carried out in equipment from Agilent (GC 6890N). The first separation was performed by a  
251 polar column VF-1701 MS (I.D 0.25 mm; Film thickness 0.25 $\mu\text{m}$ ; length 30m) followed by a  
252 second column apolar DB1 (I.D 0.25 mm; Film thickness 0.25 $\mu\text{m}$ ; length 1.5m) to promote the  
253 second dimension of separation. The modulation was performed by a cryogenic modulator from  
254 Zoex Corporation (USA) at each 12s. Compounds were identified by the coupled MS detector  
255 (5975B). The use of a polar column first, followed by the less polar column favors the separation  
256 of oxygen and nitrogen containing compounds, widely present in bio-oils.<sup>28</sup> The temperature  
257 program was set as follows: first oven (first column) from at 50 $^{\circ}\text{C}$  to 300  $^{\circ}\text{C}$  with a ramp of 1.75  
258  $^{\circ}\text{C}/\text{min}$ , then to 320 $^{\circ}\text{C}$  with a ramp of 1.8  $^{\circ}\text{C}/\text{min}$ . The second oven goes from 50  $^{\circ}\text{C}$  to 320  $^{\circ}\text{C}$  at  
259 1.8  $^{\circ}\text{C}/\text{min}$ . The samples concentration was the same as described for GC-MS analyses.

260 The solid products obtained after reaction (chars and post-reaction catalyst) were analyzed  
261 by x-ray fluorescence and elemental analysis.

## 262 3 RESULTS AND DISCUSSION

### 263 3.1 Contaminants characterization.

264 IR spectra of the dried paints and varnish (Fig. S1) showed that the varnish, white and  
265 yellow paints exhibited the main vibration bands of polymethylmethacrylate (PMMA), a polymer  
266 commonly used in acrylic paint formulation<sup>29</sup>.

267 The volatile matter of varnish and paints and the mineral elements present in their ashes  
268 analyzed by XRF are presented in Table 2. The elements with concentrations smaller than 1% were  
269 omitted. It is noteworthy to mention that XRF was used as semi-quantitative analysis, aiming to  
270 identify the main inorganic elements present in samples.

271 Table 2 - Volatile matter and mineral elements (analyzed by XRF) of paints and varnish

wt. %	Varnish	White paint	Yellow paint	Blue paint
Volatile matter	68	58	52	51
Al	4	2	-	3
Ba	-	-	51	-
Ca	33	-	7	31
Fe	3	-	7	-
K	1	-	-	-
Na	3	-	1	-
S	-	-	7	-
Si	17	3	-	4
Ti	2	66	18	33

272

273 The presence of these elements agrees with the mineral pigments commonly used in paints  
 274 formulation. For example, titanium is found predominantly in the white paint and can be related  
 275 to TiO<sub>2</sub>, a usual pigment in white paints. Similarly, BaSO<sub>4</sub> and iron oxides provide colors such as  
 276 white and yellow<sup>30, 31, 32</sup>. Ca was found in high amounts in the varnish and blue paint, it can be  
 277 assigned to the presence of CaCO<sub>3</sub>, which is a common filler used for coating materials<sup>33</sup>. This  
 278 was supported by XRD analyses (Table 3) which allowed identifying the main crystalline phases  
 279 present in the samples. The phases were very well crystallized, with intense and thin diffraction  
 280 lines suggesting large crystallites. Based on reflection lines broadening, the crystallite sizes of the  
 281 different phases identified ranged from 35 to 90 nm.

282 Table 3 - Crystalline phases found in contaminants dried at 100°C

Varnish	White paint	Yellow paint	Blue paint
CaCO <sub>3</sub> (calcite)	TiO <sub>2</sub> (rutile)	BaSO <sub>4</sub> (baryte)	TiO <sub>2</sub> (rutile)
		TiO <sub>2</sub> (rutile)	CaCO <sub>3</sub> (calcite)
		FeO(OH) (Goethite)	

283 In addition to the wood impregnated with the commercial paints and varnish, model  
 284 contaminated samples were also prepared using the clean beech wood and impregnating with 5  
 285 wt.% (on dry basis) of TiO<sub>2</sub> (rutile phase), CaCO<sub>3</sub> or BaSO<sub>4</sub>. The procedure used was the same as  
 286 described to prepare the samples with biomass and paints/varnish. The main properties of clean  
 287 beech wood chips are summarized in Table 4.

Table 4 - Properties of beech wood

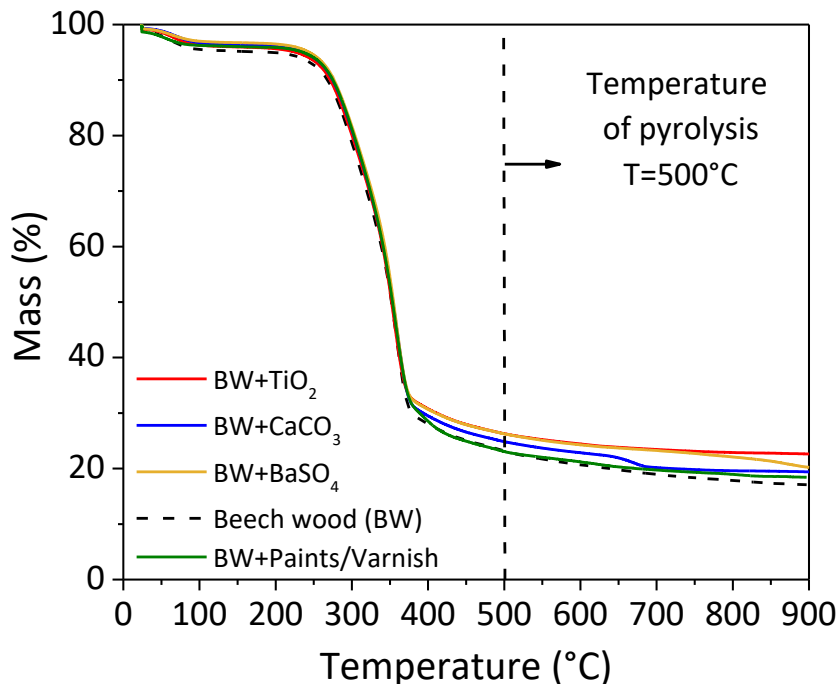
Property	Beech wood (BW)
Bulk density ( $\rho_{bulk}$ , kg/L)	0.31
Elemental analysis (wt. %)	
C	50.3 $\pm$ 0.2
H	5.4 $\pm$ 0.2
N	0.1 $\pm$ 0.04
O (by difference)	44.2 $\pm$ 0.3
Higher Heating Value (MJ/kg)	19.3 $\pm$ 0.3
Ash content (wt. %)	0.9 $\pm$ 0.1

289 The higher heating value (HHV) was calculated from the elemental analysis using the equation  
 290 proposed by Channiwala and Parikh <sup>34</sup>.

$$291 \quad \text{HHV} = 0.3491[\text{C}] + 1.1783[\text{H}] - 0.1034[\text{O}] - 0.0151[\text{N}] - 0.0211[\text{ASH}]$$

292 The calculated HHV is expressed in MJ/Kg and [C], [H], [N], [O] and [ASH] are expressed in  
 293 mass percentages on dry basis. This equation is valid for the specific range of values, i. e. C: 0.00  
 294 – 92.25 %; H: 0.43 – 25.15%; O: 0.00 – 50.00%; N: 0.00 – 5.60%; Ash: 0.00 – 71.40%.

295 Thermal gravimetric analysis (TGA) under inert atmosphere were performed to check if the  
 296 contaminants deposited on the wood particles have an impact on the degradation of biomass.  
 297 Figure 2 shows the mass loss profiles of clean and impregnated beech wood.



298  
299 Figure 2 - Mass loss profiles for clean and impregnated wood under N<sub>2</sub>

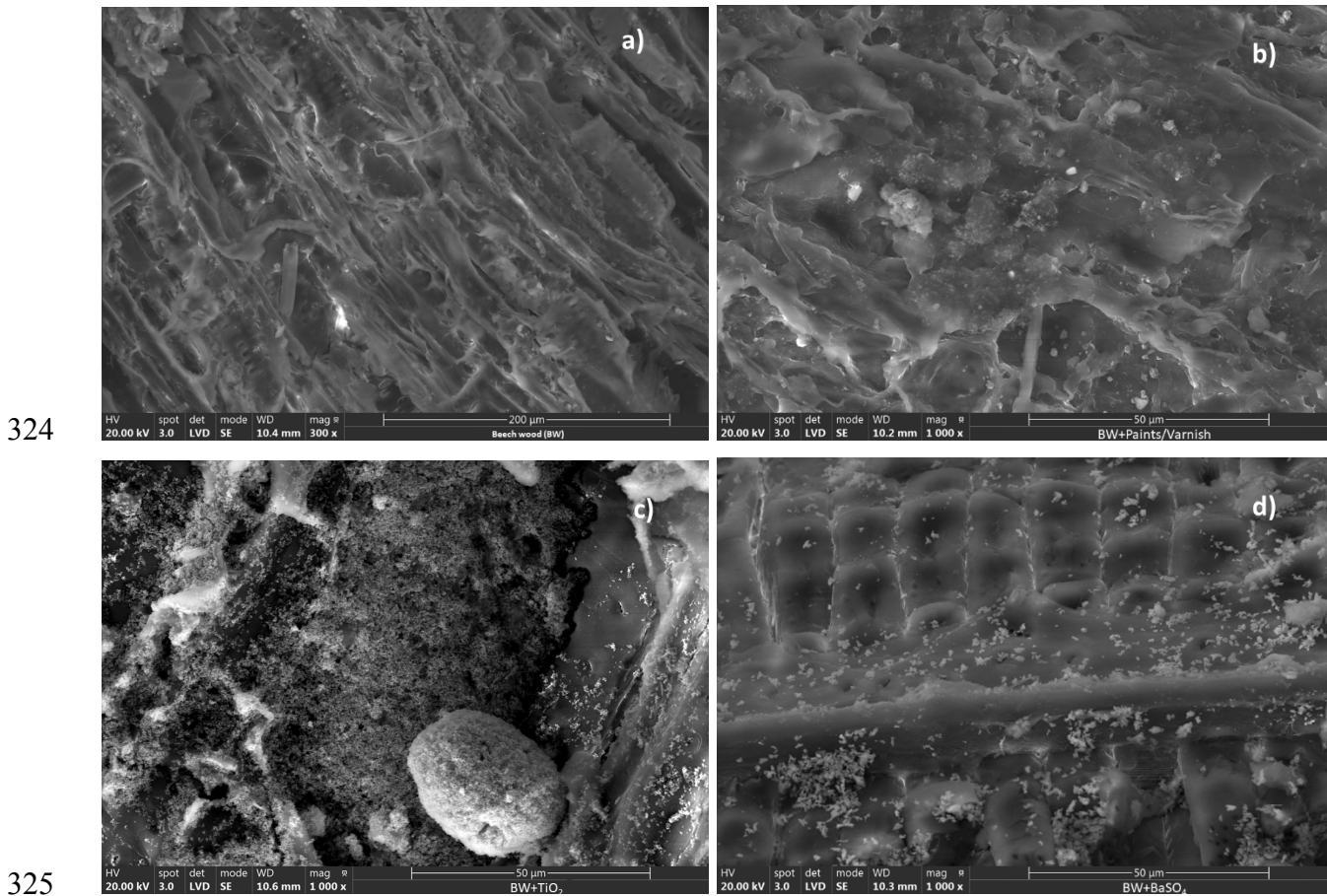
300

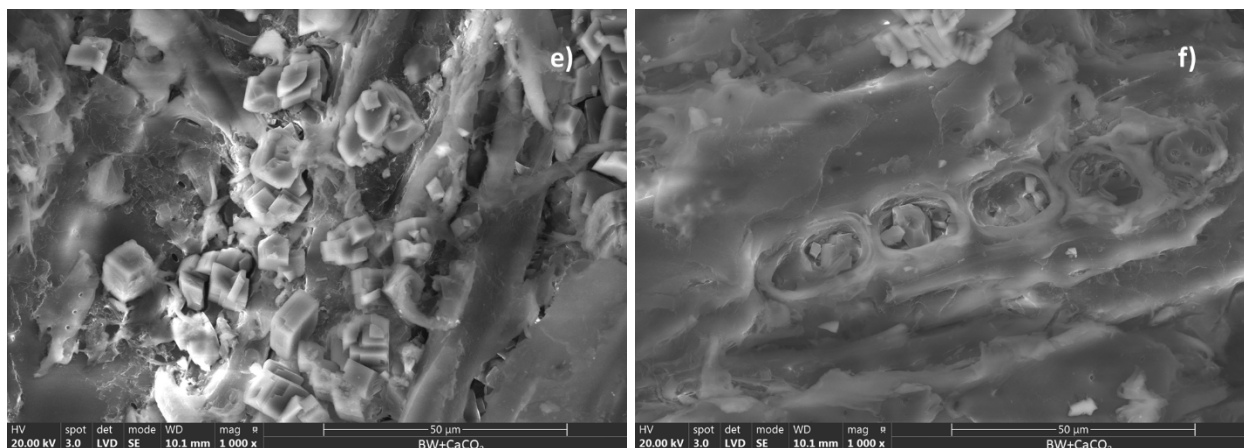
301 All samples showed similar TG profiles up to  $\approx 370$  °C. Between room temperature and 150°C,  
 302 the mass loss was related to water desorption (4-5 wt.%). Between 250 and 370°C, a large mass  
 303 loss ( $\approx 61$  wt. %) can be assigned to the degradation of wood into its volatile components<sup>35, 36, 37</sup>,  
 304 while the final remaining mass corresponds to the non-volatile components of the wood (chars).  
 305 From 370°C the curves exhibited small differences between samples, and at the pyrolysis  
 306 temperature (500 °C) the total mass loss observed varied from 77% for clean beech wood and  
 307 beech wood impregnated with paints/varnish to approximately 74% for the wood impregnated with  
 308 TiO<sub>2</sub>, CaCO<sub>3</sub> and BaSO<sub>4</sub>. Since TiO<sub>2</sub> and BaSO<sub>4</sub> are thermally very stable (MP= 1830 and 1580°C,  
 309 respectively), they will not degrade within the TGA temperature range and their mass can account  
 310 for the slightly lower overall mass loss observed with these samples. For the BW+CaCO<sub>3</sub> sample,  
 311 the small mass loss in the 650-670°C range could be related to the decomposition of CaCO<sub>3</sub> into  
 312 CaO and CO<sub>2</sub><sup>38</sup>. The similarity of TGA profiles up to  $\approx 400$ °C suggests that the presence of paints  
 313 and varnish, or their main mineral components, does not significantly modify the thermal processes  
 314 involved in wood decomposition.

315 TGA was also carried out under air to assess the ash content in the contaminated samples.  
 316 Compared to the  $\approx 0.9$  wt.% ash content found in clean wood (Table 4), the wood impregnated with

317 paints and varnish showed  $3.6 \pm 0.1\%$  of ashes while the TGA of wood impregnated with  $\text{TiO}_2$ ,  
318  $\text{CaCO}_3$  and  $\text{BaSO}_4$  showed  $5.8 \pm 0.2\%$ ,  $2.4 \pm 0.3\%$  and  $5.9 \pm 0.3\%$ , ashes content, respectively.  
319 These values are consistent with the 5 wt.% of thermally stable mineral compounds deposited on  
320 the wood, except for the sample with  $\text{CaCO}_3$ , which decomposes into  $\text{CaO}$  and  $\text{CO}_2$  during the  
321 TGA, leading ultimately to a smaller mineral content.

322 The wood chips before and after impregnation with contaminants were examined by scanning  
323 electron microscopy (SEM, Figure 3).





326  
 327 Figure 3 - SEM images of wood particles: a) clean beech wood; b) wood impregnated with  
 328 commercial paints+ varnish; c) TiO<sub>2</sub>; d) BaSO<sub>4</sub>; e) and f) CaCO<sub>3</sub>. Images: F. Simonet.

329 SEM images show the presence of particles deposited all over the wood surface. In the sample  
 330 impregnated with commercial paints and varnish, many particles appeared embedded in a layer  
 331 that could correspond to polymeric binders, plasticizers, surfactants and anti-foaming agents  
 332 constitutive of paints formulations. In the samples impregnated with TiO<sub>2</sub>, CaCO<sub>3</sub> or BaSO<sub>4</sub>, the  
 333 particles fully covered the wood surface but were densely packed in some parts. TiO<sub>2</sub> and BaSO<sub>4</sub>  
 334 formed globular particles, whereas CaCO<sub>3</sub> formed large and sharp cubic particles, some of them  
 335 filling the wood porosity, as shown in Figure 3f).

336 EDS mapping was employed to obtain information about the composition of these particles  
 337 (Figure S2). The analyses showed that the relevant elements (Ti, Ca, Ba, S) corresponded to the  
 338 particles deposited on the wood.

339 As mentioned previously, mineral species (e.g. CaCO<sub>3</sub> and BaSO<sub>4</sub>) can be used to modify the  
 340 structural properties and thermal degradation behavior of biomass<sup>22, 24, 39, 40, 41, 42</sup>. However, in  
 341 this case the biomass structure is impregnated to the core using soluble metal salt that diffuse  
 342 deeply inside the wood porosity and cell walls, leading to *in-situ* formation of the desired mineral  
 343 species. In the present study, the objective was to emulate a painted/varnished wood by coating  
 344 the wood chips with the mineral components of paints and vanish, using water suspensions of  
 345 TiO<sub>2</sub>, CaCO<sub>3</sub> and BaSO<sub>4</sub> powders. This led to the deposition of the mineral compounds on the  
 346 wood surface and in its pores, and this deposition did not significantly affect the thermal processes  
 347 leading to wood degradation into its volatile components, as shown by the TGA profiles (Figure  
 348 2).

349

### 3.2 Effect of contaminants on wood pyrolysis.

350

#### 3.2.1 Mass balance and products distribution.

351

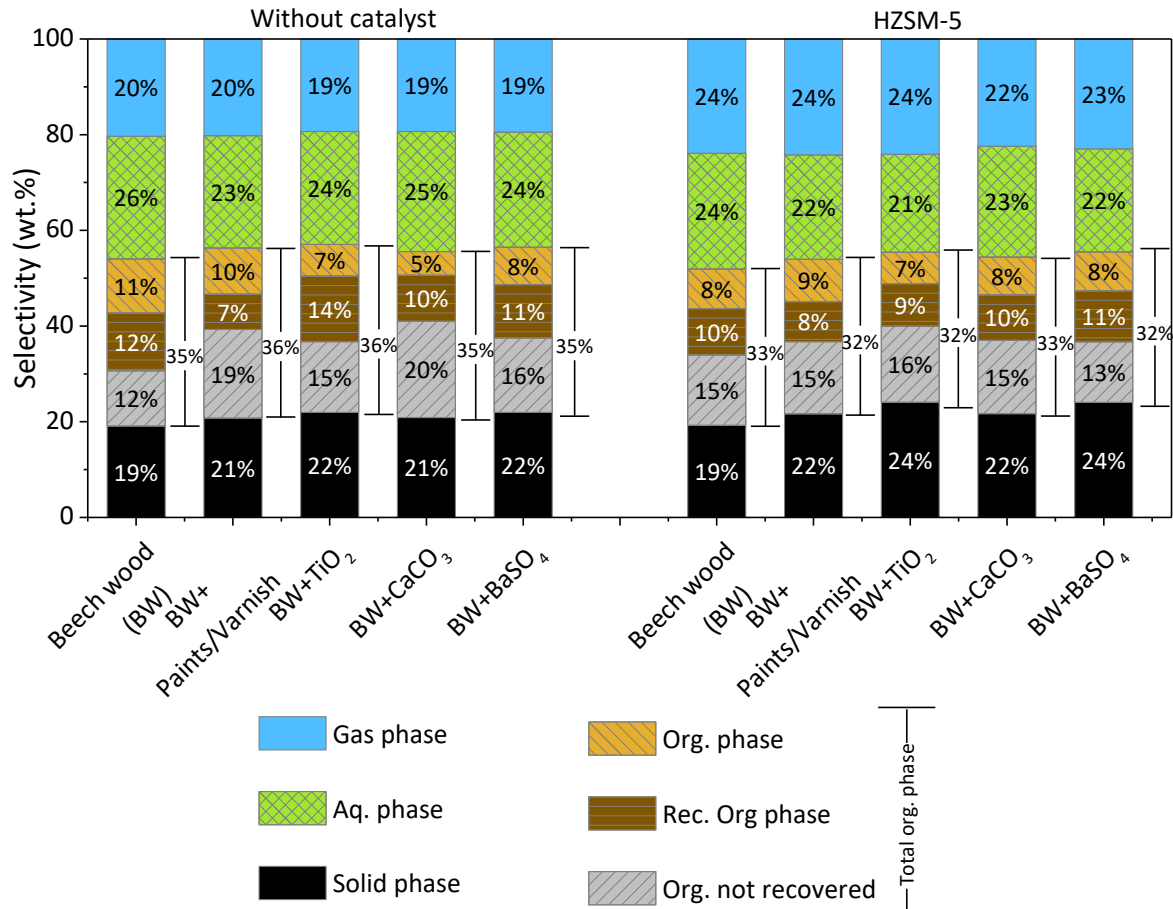
352 The impact of contaminants was assessed in absence and in presence of catalyst. Table 5  
353 shows the masses of gas, liquid and solid products and the mass balance in the experiments. The  
354 results are depicted as percentages in Figure 4.

355 Table 5 - Masses of gas, liquid and solid products and overall mass balance

Feedstock	Mass (g)			Initial mass (g) / Mass balance
	Gas phase	Liquid phase	Solid phase	
<b>Without catalyst</b>				
<b>Beech wood (BW)</b>	3.6	10.6	3.3	17.8 / 98%
<b>BW+Paints/varnish</b>	3.2	9.4	3.3	16.5 / 97%
<b>BW+TiO<sub>2</sub></b>	3.1	9.4	3.5	16.5 / 97%
<b>BW+CaCO<sub>3</sub></b>	3.1	9.7	3.4	16.7 / 97%
<b>BW+BaSO<sub>4</sub></b>	3.0	9.2	3.4	15.5 / 101%
<b>With HZSM-5 catalyst</b>				
<b>Beech wood (BW)</b>	4.1	9.8	3.3	17.8 / 97%
<b>BW+Paints/varnish</b>	3.9	8.7	3.5	16.7 / 96%
<b>BW+TiO<sub>2</sub></b>	3.6	7.7	3.6	15.4 / 96%
<b>BW+CaCO<sub>3</sub></b>	3.5	8.7	3.4	15.9 / 97%
<b>BW+BaSO<sub>4</sub></b>	3.4	7.8	3.5	15.3 / 96%

356

357 In all experiments with and without catalyst, the liquid fractions were the main products,  
358 altogether representing almost 60 wt.% of the starting feedstocks (Figure 4). In addition, the liquid  
359 phase segregated into immiscible organic and aqueous fractions after centrifugation.



361  
362 Figure 4 – Products selectivity in experiments: a) without catalyst; b) with H-ZSM-5

363 The presence of contaminants resulted in a small reduction in gas and liquid selectivity, as  
364 well as an increase in solid phase selectivity. This difference agrees with the TGA results that  
365 showed a solid residue  $\approx 3\%$  higher for contaminated samples. Considering that the most part of  
366 contaminants do not degrade at the pyrolysis temperature, they are retained in the solid phase with  
367 the chars.

368 The main liquid fraction collected was the organic phase, its total mass accounting for 35-  
369 36 % of the mass balance in experiments without catalyst, and 32-33 % in the presence of H-ZSM-  
370 5 catalyst. The yield in aqueous phase accounted for 21-26 wt. % of the total mass, with no  
371 significant differences between experiments. Overall, the yield in liquid products was close to 60  
372 wt.% in the absence of catalyst and 55 wt.% in the presence of H-ZSM-5, in agreement with the  
373 yields typically observed in thermal and ex-situ catalyzed pyrolysis, respectively.

374

375

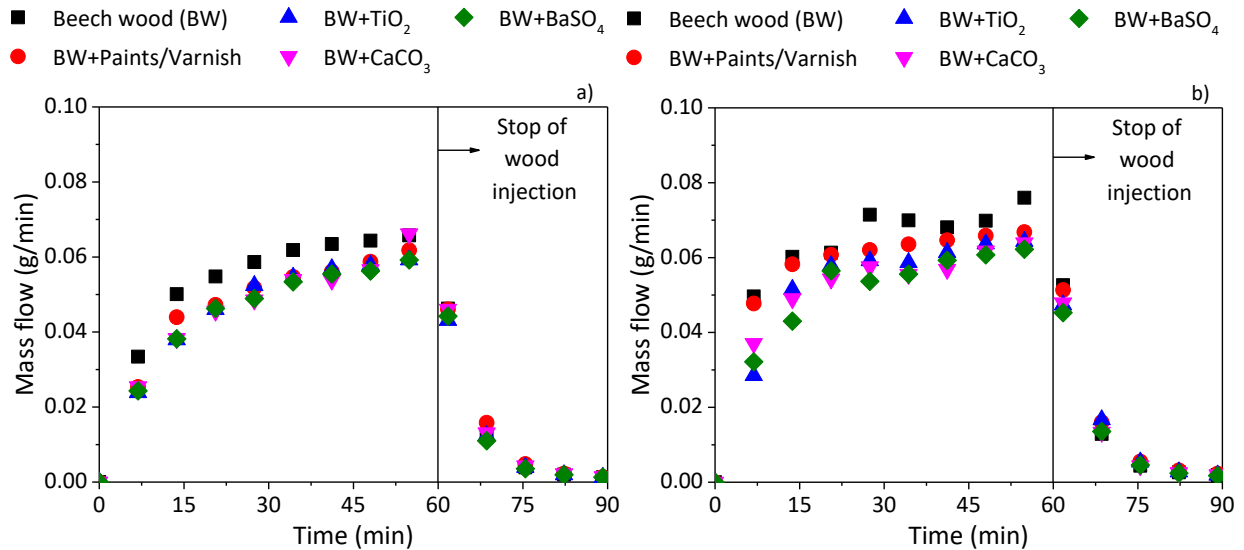
### 3.2.2 Characterization of gas phase products.

376

Figure 5 shows the production of gaseous products during the pyrolysis reaction of clean

377

and contaminated woods, in absence or presence of catalyst.



378

379

Figure 5 - Accumulated mass of gaseous products a) without catalyst and b) with HZSM-5.

380

The presence of contaminants on the wood had a modest impact on gas production with

381

time in both set of experiments. Without catalyst (Figure 5.a), the reaction performed with the

382

clean wood (black squares) produced a little more gases but this probably resulted from a slightly

383

higher mass of wood in this experiment (Table 5), because the yield of gaseous products was

384

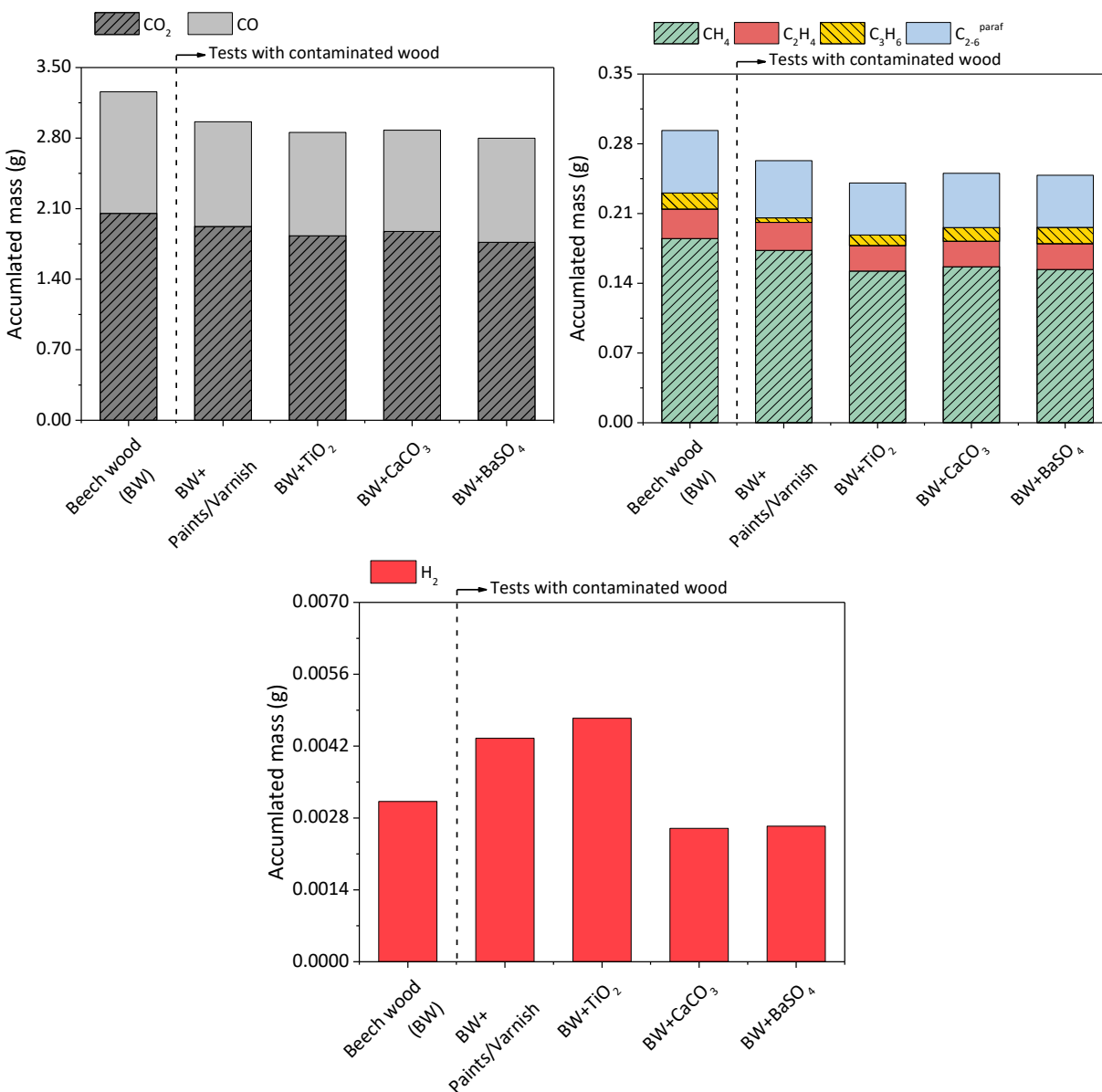
similar to that obtained in experiments with contaminated woods (Figure 4). For *ex-situ* catalytic

385

pyrolysis (Figure 5.b), the data were more scattered and these differences were even smaller. The

386

products distribution in the gas phase (without catalyst) is presented in Figure 6.



387

388  
389

Figure 6 – Gas phase composition during pyrolysis of contaminated woods (without catalyst)

390 CO and CO<sub>2</sub> were the main gaseous products, accounting for approximately 90 wt. %,  
 391 followed by CH<sub>4</sub> (~ 5 wt. % in average), light C<sub>2</sub>-C<sub>3</sub> hydrocarbons (~3 wt.%) and finally H<sub>2</sub> with  
 392 approximately 0.1 wt.%. In the presence of contaminants, there was a reduction on all compounds  
 393 compared to clean wood, except for hydrogen production which increased for BW + TiO<sub>2</sub> and BW  
 394 + paints/varnish. It has been reported in the literature <sup>43, 44</sup> that TiO<sub>2</sub> can catalyze the  
 395 dehydrogenation of propane into hydrogen and propylene, which supports the present results.  
 396 Thus, the increase in hydrogen formation observed with BW + paints/varnish could be related to  
 397 the presence of TiO<sub>2</sub>. However, reproducibility tests carried out on three experiments with clean

398 wood (Table S1 and Figure S3 in the supporting information) showed that the variations observed  
 399 on hydrogen masses are not significantly different considering the experimental error.

400 Similar trends were obtained in the presence of H-ZSM-5 catalyst (Figure S4 in supporting  
 401 information), but the production of C<sub>2</sub>-C<sub>3</sub> hydrocarbons was significantly higher than in absence  
 402 of catalyst, due to the cracking properties of H-ZSM-5.

403

### 404 3.2.3 Characterization of liquid products.

405 Table 6 presents the water content and elemental analysis of the organic phase.

406 Table 6 - Water content, elemental composition and calculated HHV of organic phase.

	H <sub>2</sub> O (%)	Composition (wt. %, on dry basis)				HHV (MJ/Kg)
		C	H	N	O*	
Without catalyst						
Beech wood (BW)	18.6 ± 0.2	65.3 ± 1.0	6.1 ± 0.4	0.6 ± 0.1	28.1 ± 1.5	27.0 ± 1.0
BW+paints/varnish	16.1 ± 1.5	67.0 ± 1.6	6.5 ± 0.1	0.8 ± 0.1	25.6 ± 1.6	28.4 ± 0.6
BW+TiO <sub>2</sub>	19.5 ± 0.5	64.0 ± 0.8	6.5 ± 0.3	0.8 ± 0.6	28.8 ± 0.9	26.9 ± 0.5
BW+CaCO <sub>3</sub>	21.0 ± 0.3	59.0 ± 1.0	8.6 ± 1.1	0.8 ± 0.5	31.6 ± 0.4	27.5 ± 0.9
BW+BaSO <sub>4</sub>	21.8 ± 1.4	66.1 ± 2.2	6.6 ± 0.4	0.8 ± 0.5	26.6 ± 2.3	28.0 ± 0.6
With H-ZSM-5						
Beech wood (BW)	11.9 ± 0.3	70.4 ± 0.9	6.6 ± 0.3	0.7 ± 0.3	22.4 ± 1.0	30.0 ± 0.2
BW+paints/varnish	9.4 ± 1.6	71.8 ± 0.9	6.7 ± 0.2	1.2 ± 1.3	20.3 ± 0.7	30.9 ± 0.5
BW+TiO <sub>2</sub>	13.8 ± 0.4	74.7 ± 1.4	6.5 ± 0.1	0.7 ± 0.2	18.1 ± 1.1	31.9 ± 0.5
BW+CaCO <sub>3</sub>	11.3 ± 0.5	70.0 ± 0.8	6.6 ± 0.2	0.7 ± 0.6	22.8 ± 0.5	29.8 ± 0.3
BW+BaSO <sub>4</sub>	14.6 ± 1.3	69.9 ± 1.7	6.1 ± 1.4	0.8 ± 0.8	23.1 ± 2.2	29.2 ± 2.0

407 \*Calculated by difference

408 Within series of experiments carried out without or with catalyst, the presence of  
 409 contaminants on the wood did not significantly modify the bio-oils composition. The presence of  
 410 contaminants generally led to a slight increase in the water content of bio-oils compared to clean  
 411 wood, except for the BW+paints/varnish sample. In contrast, the bio-oils formed in the presence  
 412 of the H-ZSM-5 catalyst clearly contained less water, more carbon and less oxygen than the  
 413 thermal bio-oils.

414 The aqueous phase was also analyzed in the experiments carried out with clean BW and  
 415 BW+paints/varnish. Table 7 gives the total organic carbon (TOC), the water content and the  
 416 elemental analysis. It is noteworthy that in this case, the CHN analyses were not corrected for the  
 417 water content.

418 Table 7 – Aqueous phase composition.

	TOC (wt.%)	H <sub>2</sub> O (%)	Composition (wt.%)			
			%C	%H	%N	%O*
<b>Without catalyst</b>						
<b>BW</b>	23.1±0.3	48.3±1.2	27.0±0.2	8.6±1.6	0.6±0.3	63.8±1.3
<b>BW+paints/varnish</b>	21.0±0.5	54.0±0.1	22.5±1.1	9.1±1.5	0.4±0.1	67.9±2.4
<b>With H-ZSM-5</b>						
<b>BW</b>	12.4±0.1	71.4±1.3	12.9±1.6	9.8±2.3	0.4±0.3	77.0±3.7
<b>BW+paints/varnish</b>	8.03±0.02	82.1±0.7	8.6±0.3	10.1±1.0	0.5±0.4	80.8±0.9

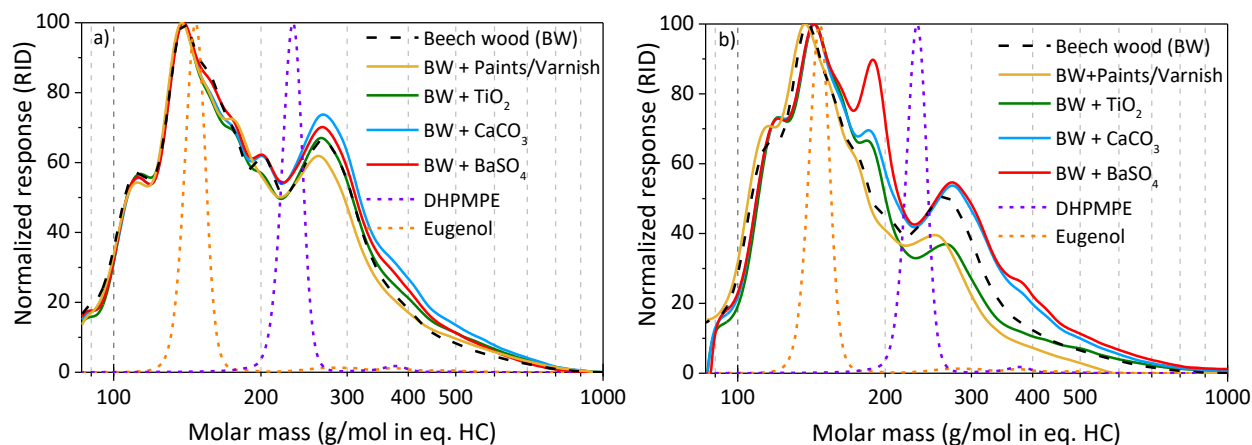
419 \*Calculated by difference

420 The TOC measurements agreed reasonably well with the carbon analysis and confirmed  
 421 that the aqueous phase was composed mainly of water, but the thermal bio-oils, however,  
 422 contained >20 wt. % of organic carbon. The effect of the catalyst appears here very important since  
 423 it allows halving the carbon content of the aqueous phase by converting a good part of the water-  
 424 soluble compounds into less polar compounds which remain in the organic phase.

425  
 426 Figure 7 shows the molar mass distributions of the organic fraction, measured by GPC.  
 427 The chromatograms were normalized to the highest peak intensity. As a matter of comparison, the  
 428 chromatograms of two reference compounds, eugenol (164 g/mol) and DHPMPE (274 g/mol) are  
 429 overlaid. DHPMPE corresponds approximately to the detection limit of GC-MS analyses, i.e.  
 430 compounds that can be vaporized and eluted at 250°C.

431 In both series of experiments without or with catalyst, four major MW peaks could be  
 432 identified, at 120, 140, 190 and 267 g/mol (in HC eq.). These MWs may be slightly under-  
 433 estimated given the deviations observed for reference compounds (Table 8), which can be assigned  
 434 to the different hydrodynamic volume of analyzed compounds compared to the hydrocarbon

435 standards used in the calibration. The peak intensities with a RI detector are also compound-  
 436 dependent and molecules with polarizable groups such as aromatics exhibit higher refractive  
 437 indices than compounds with less polarizable groups (i.e. oxygen atoms or alkyl groups)<sup>45</sup>.  
 438



439  
 440 Figure 7 - Molar mass distribution of organic phase a) without catalyst b) with H-ZSM-5.

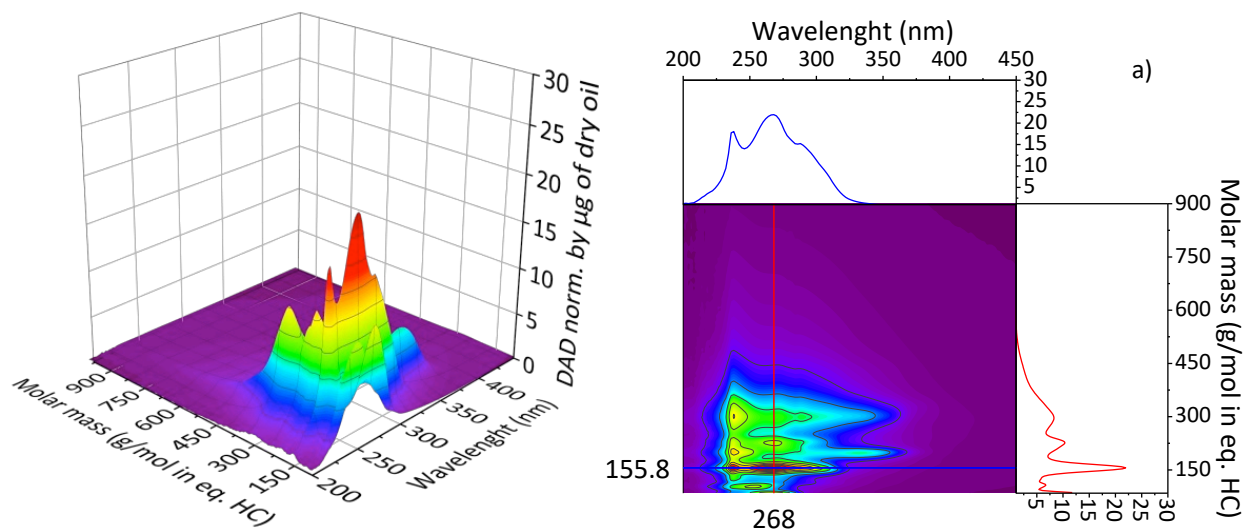
441 Without catalyst, the low MW region (below the DHPMPE peak) corresponded to 49.5 % of the  
 442 total area; this ratio increased to 55% in the presence of H-ZSM-5 (the X scale in Figure 7 being  
 443 logarithmic, the visualized areas are misleading). This translates into slightly reduced average  
 444 MWs in the presence of H-ZSM-5 (Table 8).

445 Table 8 – Weight average molecular mass of organic fraction (in HC equivalent).

	$M_w$ (g/mol in eq. HC)	
	<b>Standards</b>	
	Theoretical	Measured
Eugenol	164	147 (-10.4 %)
DHPMPE	274	234 (-14.6 %)
	<b>Organic fraction</b>	
	Without catalyst	H-ZSM-5
Beech wood (BW)	211	200
BW+paints/varnish	217	177
BW+TiO <sub>2</sub>	221	198
BW+CaCO <sub>3</sub>	228	213
BW+BaSO <sub>4</sub>	217	218

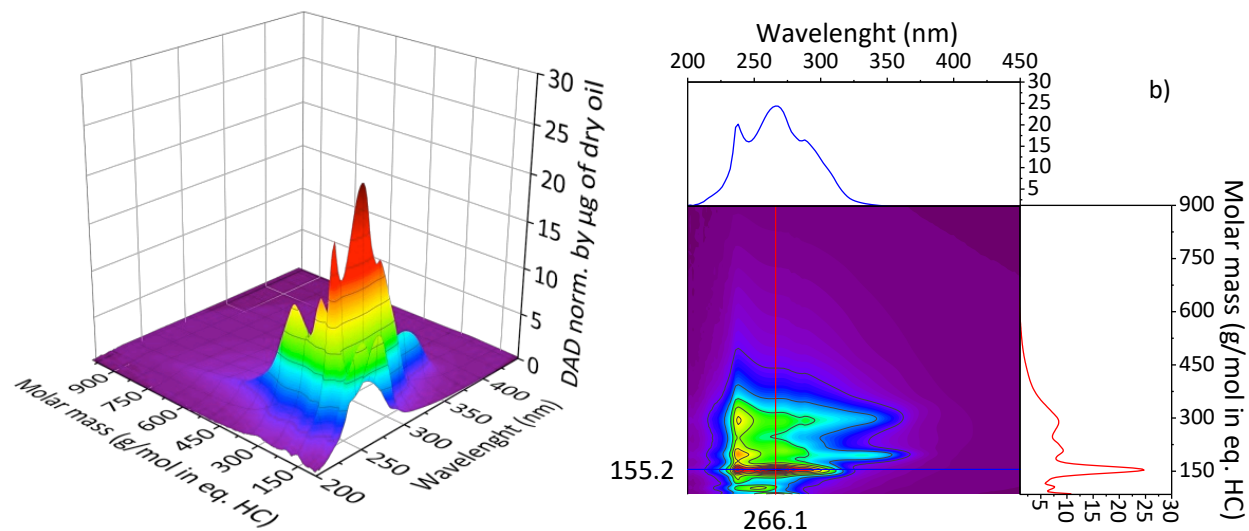
446

447 The bio-oils were also analyzed with GPC-UV-DAD to obtain a deeper insight on the  
448 nature of UV-adsorbing bonds of the dissolved compounds. Figure 8 shows the 3D plots obtained  
449 at wavelengths between 200 and 450 nm for MWs between 86 and 1000 g/mol. The peaks  
450 intensities were normalized per  $\mu\text{g}$  of dry bio-oil to correct the detector response for the small  
451 differences in samples dilution. Given the modest impact of mineral contaminants, only the results  
452 for the organic phase obtained with BW and BW+paints/varnish are shown. For all samples, the  
453 most intense absorption peak was centered around 267 nm. Absorption in this region is assigned  
454 to aromatics and unsaturated conjugated compounds. The presence of contaminants on the wood  
455 had no significant impact on the surface shape. For the sample obtained with contaminated wood  
456 and H-ZSM-5 (Figure 8c), the maximum wavelength and molar mass peaks were centered in the  
457 same region (266 and 155, respectively). However, the MW distribution was clearly narrower than  
458 in absence of catalyst, with lower intensities above 200 g/mol. Therefore, the H-ZSM-5 catalyst  
459 appears to promote a deeper depolymerization of aromatic and/or unsaturated conjugated  
460 components of bio-oils.

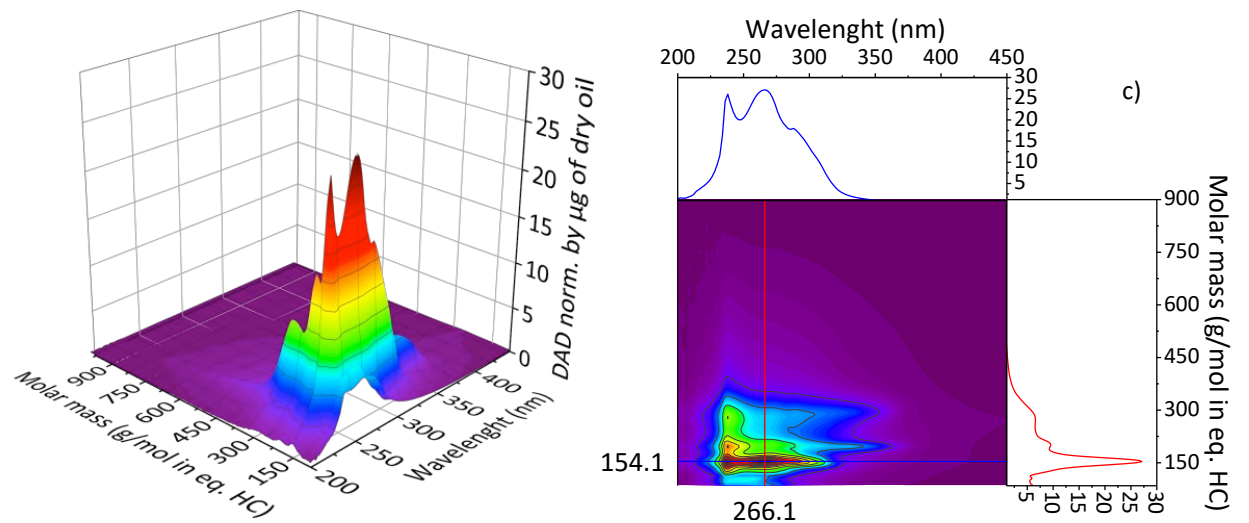


461

462



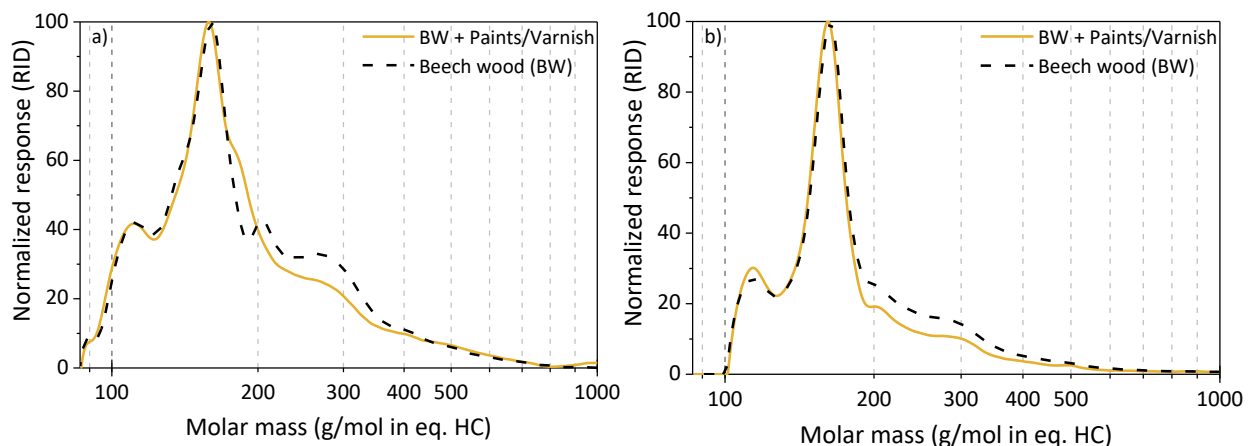
463



464 Figure 8 - GPC-DAD chromatograms of organic fractions obtained from: a) Beech wood without  
465 catalyst; b) BW+paints/varnish without catalyst; c) BW+paints/varnish with H-ZSM-5.

466

467 The molar mass distributions of the aqueous phases obtained with clean BW and  
468 BW+paints/varnish pyrolysis are shown in Figure 9. The composition of aqueous phase is  
469 essentially different from that of the organic phase, as will be shown later, which implies that the  
470 compounds present in the aqueous phase have probably different hydrodynamic volumes.  
471 Therefore, the measurements obtained for the organic and aqueous phases cannot be compared  
472 directly, but the aqueous phases can be compared with each other.

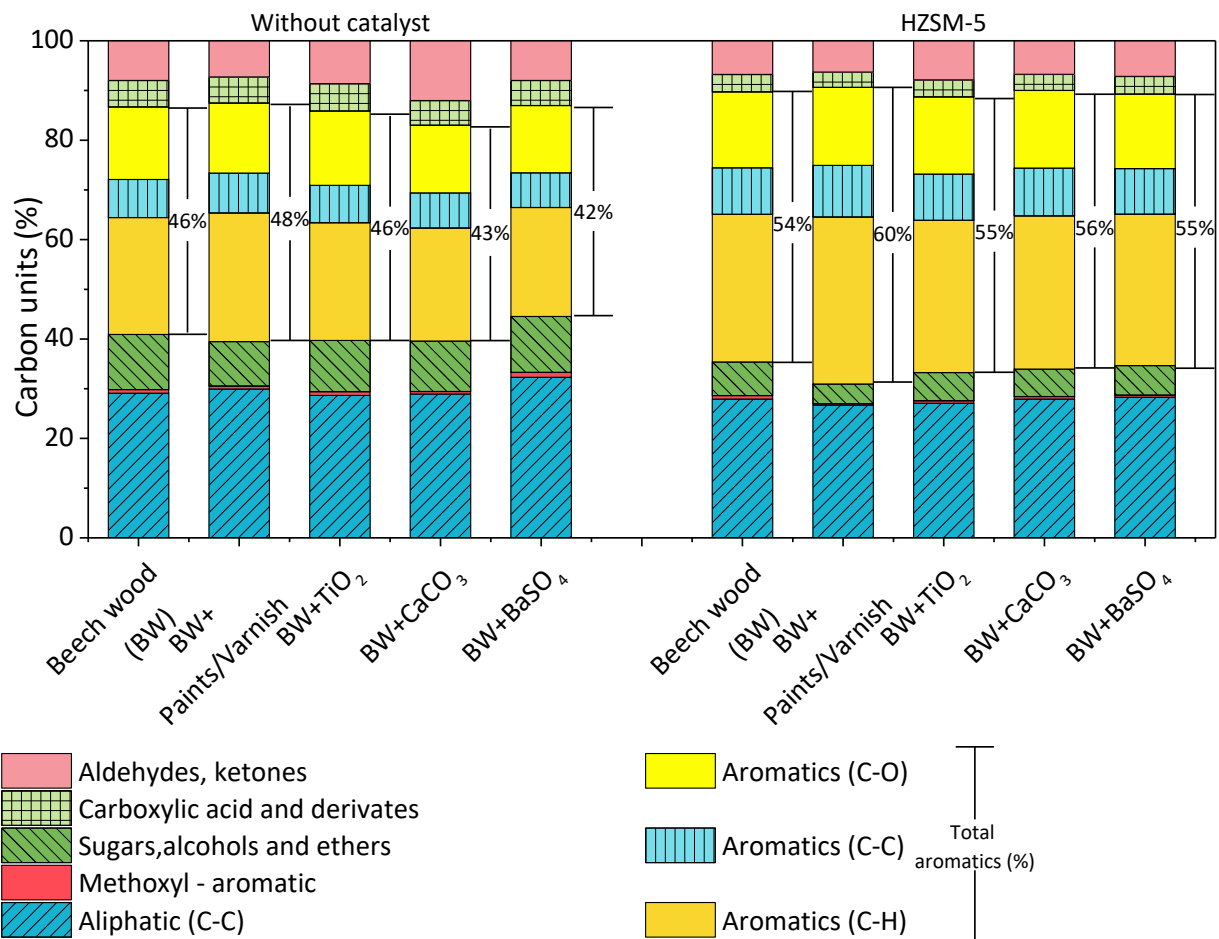


473  
 474 Figure 9 - Molar mass distribution of aqueous phase a) without catalyst b) with H-ZSM-5

475 The molar mass distribution of the aqueous phase exhibited the most intense peak at  $\approx 160$   
 476 g/mol (in eq. HC) and was narrower than that of the organic phase. Similarly, Hoekstra et al.<sup>45</sup>  
 477 observed that the aqueous phase separated from a bio-oil contains mostly low MW compounds.  
 478 Overall, the shapes of the curves were similar in experiments with clean and contaminated wood.  
 479 However, in the presence of H-ZSM-5 the peaks intensity above 200 g/mol was clearly lower,  
 480 indicating that the aqueous phases contained less compounds above this MW than in absence of  
 481 catalyst.

482  
 483  $^{13}\text{C}$ -NMR is a very useful technique for characterizing bio-oils, since it provides a global  
 484 analysis of any fraction that is soluble in the chosen solvent, independently of MWs or volatility,  
 485 and detailed information regarding the functional groups of bio-oils components. The chemical  
 486 shifts ranges attributed to the main functional groups are detailed in Table S2 (supporting  
 487 information). The  $^{13}\text{C}$ -NMR carbon distribution of functional groups in the organic fraction  
 488 obtained with each wood sample, with or without catalyst, is depicted in Figure 10.

489

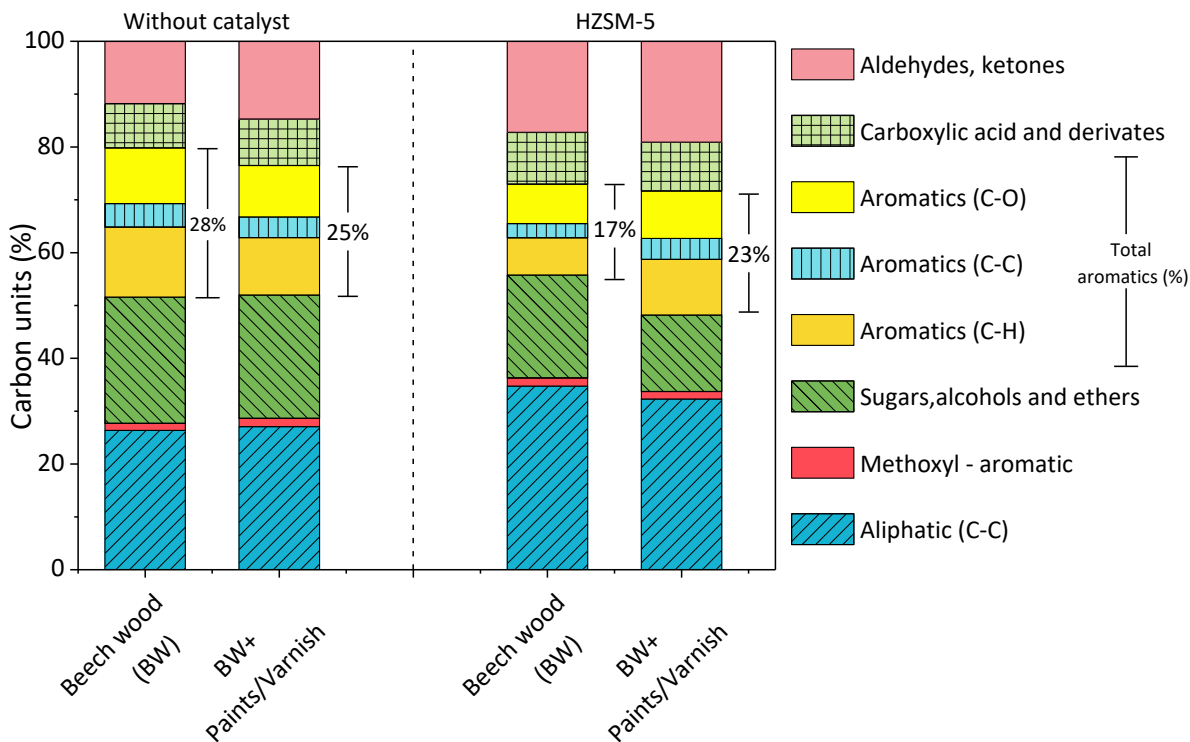


490  
491 Figure 10 – <sup>13</sup>C-NMR functional groups distribution in organic phases obtained a) without  
492 catalyst and b) with HZSM-5

493 The presence of contaminants on wood did not significantly modify the functional groups  
494 distribution in bio-oils, within the same series of experiments (with or without catalyst). The effect  
495 of H-ZSM-5 catalyst on the bio-oils composition, however, was confirmed through the increased  
496 yield of aromatics (54-60 % vs. 42-46 % without catalyst), whereas the yield of sugars, alcohols  
497 and carboxylic compounds decreased.

498 Similarly, the aqueous fractions were analyzed by <sup>13</sup>C-NMR (Figure 11).

499



500 Figure 11 –  $^{13}\text{C}$ -NMR functional groups distribution of aqueous phases obtained in experiments  
 501 without catalyst or with H-ZSM-5.  
 502

503 Comparing Figure 10 and Figure 11 shows that the overall composition of aqueous phases  
 504 was very different from the organic phase's composition. The aqueous phases exhibited a smaller  
 505 concentration of aromatic carbon units (with a high ratio of C-O/C-H+C-C aromatic bonds  
 506 indicating highly oxygenated compounds) and a higher concentration of polar carbon units, such  
 507 as sugars, alcohols, ethers, aldehydes and ketones. Compounds bearing these polar groups are  
 508 expected to show a higher affinity with water and, therefore, to partition preferentially in the  
 509 aqueous phase during the phase separation process. The TOC content of aqueous phases was  
 510 shown previously to decrease strongly in the presence of H-ZSM-5 catalyst (Table 7): this  
 511 translates in a different distribution of functional groups, with more small aliphatic compounds  
 512 (probably also bearing aldehydes, ketonic groups) and less aromatics. This suggests that the  
 513 catalyst converts the aromatic oligomers present in the pyrolysis vapors into smaller and less polar  
 514 aromatic compounds that are more soluble in the organic phase than in the aqueous phase.

515 GC-MS was employed to obtain a more detailed insight on the composition of bio-oils.  
 516 Given the complexity of the samples (around 600 different compounds were identified with good  
 517 similarity indexes throughout all analyses performed), the calibration of each compound is not

518 possible. In addition, some peaks are not fully separated and resolved, resulting in less accurate  
 519 integration. However, the comparison between peak areas of similar compound families is valid  
 520 and can highlight composition variations due to the presence of contaminants <sup>46, 47, 48, 49</sup>.

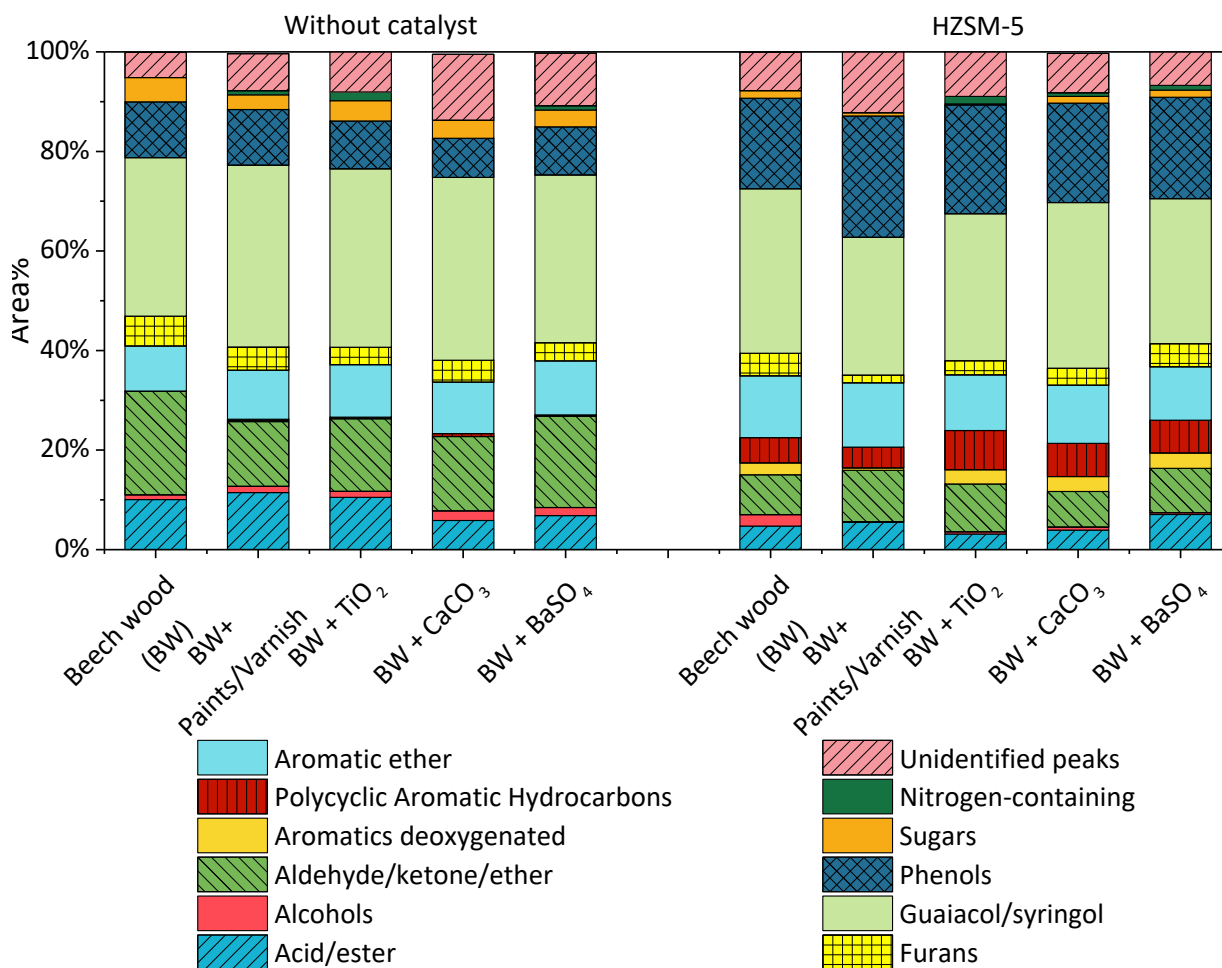
521 Additionally, the GC-MS technique is limited to the analytes that can be volatilized without  
 522 thermal decomposition and elute at 250°C (maximum temperature of the analytical column). As  
 523 an example, the peak of DHPMPE (274 g/mol, solid at room temperature) used as reference  
 524 compound in GPC analyses elutes at the final GC temperature program (250°C). Higher MW or  
 525 boiling points compounds are therefore excluded from this analysis.

526 Compounds were grouped into families based on similar functional groups (Table 9).

527 Table 9 – GC-MS compound families and examples

Compound family	Examples
Acid/ester	Organic acids (acetic, propanoic, butanoic...), vinyl butyrate
Alcohols	1,2-ethanediol, cyclopropyl carbinol
Aldehyde/ketone/ether	1-hydroxy-2-propanone, cyclopentenones
Aromatics	benzene, xylene, styrene
Aromatic ether	1,2,4-trimethoxybenzene, 3,4-dimethoxytoluene
Furans	2(5H)-furanone, furfural, 5-hydroxymethylfurfural
Guaiacol/syringol	2,6-dimethoxy-phenol, guaiacol, 2,6-dimethoxy-4-(2-propenyl)-phenol
Nitrogen-containing	6-methyl-4(1H)-pyrimidinone, 3-methylpyridazine
Polycyclic aromatic hydrocarbons (PAH)	indane, naphthalenes,
Phenols	catechols, alkyl-phenols
Sugars	levoglucosan, DL-arabinose, 2,3-anhydro-d-mannosan

528 The selectivity for families of compounds of the organic phases obtained with the different  
 529 feedstocks and experimental conditions are presented in Figure 12.



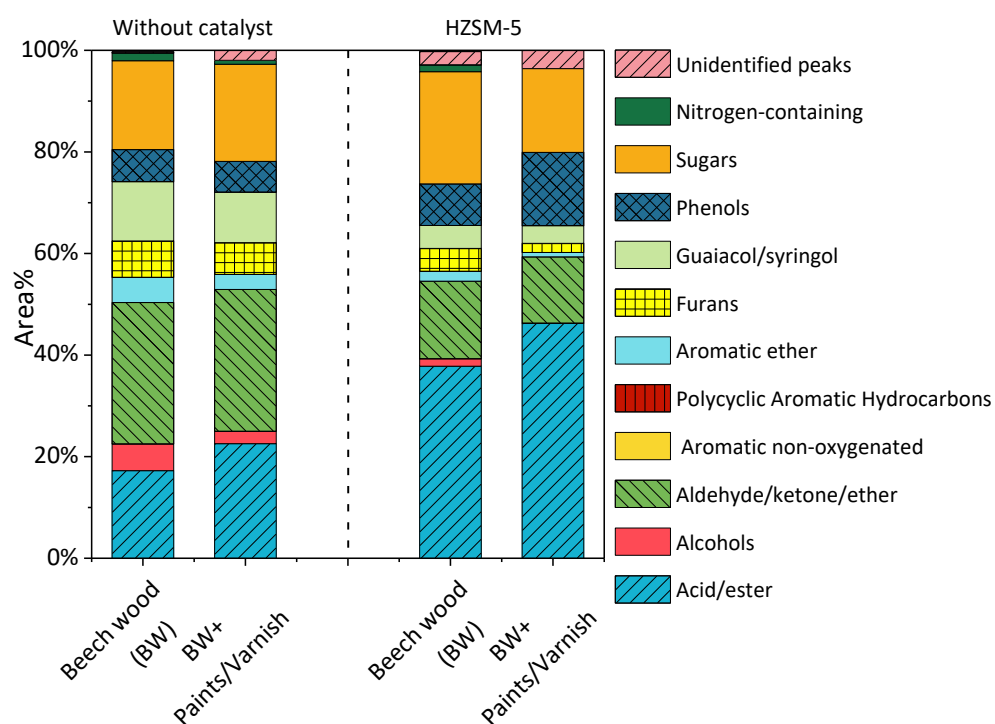
530  
 531 Figure 12 - Relative areas of compound families in organic fractions analyzed by GC-MS. a)  
 532 Without catalyst and b) with HZSM-5

533 These results fully support the general trends observed with  $^{13}\text{C}$ -NMR. In absence of  
 534 catalyst, the organic phase contained essentially oxygenated aromatic compounds derived from  
 535 lignin, such as guaiacols, phenols, ethers, and the presence of contaminants did not induce strong  
 536 differences in the products distribution. The main compound found was generally 2,6-dimethoxy-  
 537 4-(2-propenyl)-phenol, accounting for approximately 8% of the total area.

538 Fully deoxygenated aromatic and polyaromatic compounds were found only after ex-situ  
 539 catalytic treatment, highlighting the effect of H-ZSM-5 catalyst in promoting the dehydroxylation,  
 540 decarbonylation and decarboxylation reactions leading to the removal of oxygenated groups. With  
 541 H-ZSM-5 and the BW+paints/varnish sample, however, a significant decrease in the amounts of  
 542 fully deoxygenated compounds could be noticed, which was not observed for contaminated woods  
 543 impregnated with  $\text{TiO}_2$ ,  $\text{CaCO}_3$  or  $\text{BaSO}_4$ . This suggests that the polymeric organic compounds

544 present in commercial paints or varnish (i.e. polymethylmethacrylate or other organic additives),  
 545 observed in IR spectra and SEM images, could lead to partial catalyst deactivation affecting its  
 546 deoxygenation functionality, but not its cracking functionality. This could be related to their  
 547 decomposition into coke precursors small enough to diffuse into the micropores of H-ZSM-5 and  
 548 to poison the most acidic sites.

549 Similarly, the selectivity for families of compounds of the aqueous phases obtained from  
 550 clean BW and BW+paints/varnish is depicted in Figure 13.



551  
 552 Figure 13 - Relative areas of compound families in aqueous fractions analyzed by GC-MS.

553 The aqueous phases contained essentially polar compounds (acids, esters, ketones, sugars).  
 554 The aqueous phase composition changed more significantly in the presence of catalyst than did  
 555 the organic phase composition. Without catalyst, the most abundant organic product was 1,6-  
 556 anhydro- $\beta$ -D-glucopyranose (also named levoglucosan), accounting for  $\approx$ 15% of the total peaks  
 557 area, whereas with H-ZSM-5 acetic acid was the main product, with more than 35% of the total  
 558 area. Indeed, the zeolite is known for its ability to reduce the amounts of sugars in bio-oils<sup>50, 51,</sup>  
 559<sup>52</sup>. It should be mentioned that in Figure 13 the peak areas are normalized to the total peaks area  
 560 in GC-MS, but they actually correspond to very different TOC amounts in the aqueous phases, cf.  
 561 Table 7.

562 Two-dimensional GCxGC analyses (Table S3 and Figures S5 and S6 in the supporting  
563 information) also confirmed these trends.

564 In summary, the characterizations of liquid products obtained by thermal pyrolysis, and  
565 more specifically the organic phases, show that the presence of evaluated contaminants on the  
566 wood did not impair the quality of the final bio-oil. When ex-situ catalytic treatment of the vapors  
567 using H-ZSM-5 catalyst was applied, the composition of bio-oils was improved, in terms of lower  
568 oxygen and water contents, reduction in high MW oligomers content and decrease of sugars and  
569 carboxylic acids, which confer bio-oils their acidic properties. The deposition of commercial  
570 paints/varnish on the wood appeared to partially hinder the formation of deoxygenated compounds,  
571 but this effect was not related to the main mineral compounds present in the paints and varnish.

### 572 3.2.4 Chars and post-reaction catalysts characterization

573 The yields of solid products deposited at the reactor outlet were similar after each pyrolysis  
574 reaction (Table 5). TGA of chars under N<sub>2</sub> showed that the mass loss was <5 wt.% in the 150-  
575 500°C temperature range (Fig. S7 in supporting information), which suggests that most of the  
576 volatile compounds were extracted from the wood during the pyrolysis process. XRD of the chars  
577 (Fig. S8 in supporting information) also revealed that the mineral phases (TiO<sub>2</sub>, CaCO<sub>3</sub>, BaSO<sub>4</sub>)  
578 initially deposited on the wood were found unmodified in the chars after pyrolysis. Table 10  
579 compares the elemental analyses and the calculated HHV of the chars.

580 Table 10 - Elemental analysis of chars obtained after pyrolysis of different woods

Feedstock	Mass composition, on dry basis (wt.%)				HHV (MJ/Kg)
	C	H	N	O*	
<b>Beech wood (BW)</b>	82.3±0.5	3.0±0.4	0.3±0.03	14.4±0.5	30.7±0.4
<b>BW+paints/varnish</b>	75.2±0.6	2.7±0.3	0.3±0.1	21.9±0.8	27.1±0.6
<b>BW+TiO<sub>2</sub></b>	64.2±1.5	2.3±0.01	0.2±0.02	33.3±1.4	21.7±0.7
<b>BW+CaCO<sub>3</sub></b>	71.1±0.5	2.6±0.01	0.3±0.04	26.1±0.6	25.1±0.3
<b>BW+BaSO<sub>4</sub></b>	65.4±0.5	2.3±0.1	0.2±0.01	32.2±0.6	22.2±0.4

581

582 The chars obtained from contaminated woods contained less carbon and more oxygen than  
 583 the char from clean wood. This behavior can be related to the presence of mineral species, which  
 584 increases the incombustible fraction of chars and consequently results in lower HHVs. In an  
 585 eventual process integration, a lower HHV will result in less energy that can be recovered from  
 586 this by-product.

587 In *ex-situ* catalytic experiments, the chars (Table 11) and the post-reaction H-ZSM-5  
 588 catalyst (Table 12) were also analyzed by XRF, aiming to assess a possible transfer of pollutants  
 589 from the wood to the catalyst (placed after the pyrolysis zone and immediately after the frit that  
 590 collects the chars, *cf.* Figure 1), which could impact the catalytic activity.

591 Table 11 – Chemical composition of chars analyzed by XRF

Feedstock	Element concentration* (wt.%)					
Beech wood (BW)	Ca	K	Mn	Mg		
	8.9	3.7	0.7	0.5		
BW+Paints/varnish	Ti	Ca	K	Fe	Si	Ba
	15.5	8.1	2.7	1.3	0.9	0.6
BW+TiO <sub>2</sub>	Ti	Ca	K			
	52.5	2.6	1.9			
BW+CaCO <sub>3</sub>	Ca	K				
	28.1	2.2				
BW+BaSO <sub>4</sub>	Ba	S	Ca	K	Mg	
	23.0	6.7	4.1	2.7	0.5	

592 \*Elements with concentrations smaller than 0.5% are not shown

593 Compared to the char formed from clean wood, the chars from contaminated woods  
 594 contained larger amounts of the inorganic pollutants originally impregnated on the biomass.

595 Table 12 -XRF analyses of fresh and post-reaction H-ZSM-5 catalyst after pyrolysis of different  
 596 feedstocks

Feedstock	Elements	Concentration* (wt.%)							
		Si	Al	P	Ca	Cl	Ti	Fe	Cr
<b>H-ZSM-5 catalyst before reaction</b>									
-		33.68	0.78	0.22	0.17	0.10	0.04	0.02	0.01
<b>H-ZSM-5 catalyst after reaction</b>									
<b>BW+paints/varnish</b>		35.79	0.78	0.21	0.18	0.10	0.05	0.02	0.01
<b>BW+TiO<sub>2</sub></b>		37.19	0.82	0.19	0.17	0.09	0.05	0.02	0.01

<b>BW+CaCO<sub>3</sub></b>	36.17	0.80	0.21	0.18	0.09	0.04	0.02	0.01
<b>BW+BaSO<sub>4</sub></b>	35.35	0.77	0.21	0.17	0.10	0.04	0.02	0.01

597 \*-Elements with concentrations smaller than 0.01% are not shown

598 XRF analyses are only semi-quantitative, however they allow an accurate comparison of  
599 samples with similar properties. The concentration of inorganic pollutants (Ti, Ca, Ba and S) in  
600 the catalyst was not modified after pyrolysis of contaminated woods. These results show that the  
601 mineral contaminants remained in the chars and were not transferred to the catalyst, which  
602 validates the choice of an ex-situ catalytic configuration for the reactor. The catalyst and the  
603 biomass are not in direct contact and the contaminants can be removed from the system with the  
604 char.

#### 605 4 CONCLUSIONS

606 The main conclusions of this study can be summarized as follows:

- 607 • Commercial acrylic paints and varnish deposited on clean beech wood had no significant  
608 influence on the composition of bio-oils prepared by thermal pyrolysis of this contaminated  
609 wood.
- 610 • The main mineral components of paints and varnish were TiO<sub>2</sub>, CaCO<sub>3</sub> and BaSO<sub>4</sub>, they  
611 essentially remained in the solid char residues formed after pyrolysis.
- 612 • When ex-situ catalytic treatment of the pyrolysis vapors in the presence of HZSM-5  
613 catalyst was applied, the composition of bio-oils originating from both clean and  
614 contaminated woods was improved in terms of lower oxygen and water contents, lower  
615 high MW oligomers content and decrease of carboxylic acid groups.
- 616 • The mineral components of paints and varnish were not transferred to the catalyst.  
617 However, their polymeric organic components might be pyrolyzed into coke precursors,  
618 leading to an inhibition of the catalyst deoxygenation properties.

619

620 **Supporting information:** ATR-FTIR spectra of paints and varnish; reproducibility of H<sub>2</sub>  
621 production; gaseous products composition in pyrolysis of contaminated woods with H-ZSM-5  
622 catalyst; <sup>13</sup>C NMR chemical shifts; compound families in GCxGC-MS analyses of organic and  
623 aqueous phases; TGA and XRD of chars obtained from clean and contaminated woods.

624

## 625 Acknowledgements

626  WASTE2ROAD project has received funding from the European Union's Horizon 2020  
627 research and innovation programme under grant agreement N° 818120.

628 The authors thank Chantal Lorentz and Ruben Checa for their valued help with NMR, GCxGC,  
629 CHONS and GPC analyses, and France Simonet for SEM/EDX images and analyses.

630

## 631 References

632 (1) Pinho, A. de R.; de Almeida, M. B. B.; Mendes, F. L.; Ximenes, V. L.; Casavechia, L. C.  
633 Co-Processing Raw Bio-Oil and Gasoil in an FCC Unit. *Fuel Processing Technology* **2015**, *131*,  
634 159–166. <https://doi.org/10.1016/j.fuproc.2014.11.008>.

635 (2) European Commission. *Implementation of EU Waste Legislation, Including the Early*  
636 *Warning Report for Member States at Risk of Missing the 2020 Preparation for Re-*  
637 *Use/Recycling Target on Municipal Waste*; COM(2018) 656 final; 2018.

638 (3) European Commission; Directorate-General for Environment. Waste Framework  
639 Directive [https://ec.europa.eu/environment/topics/waste-and-recycling/waste-framework-](https://ec.europa.eu/environment/topics/waste-and-recycling/waste-framework-directive_en)  
640 [directive\\_en](https://ec.europa.eu/environment/topics/waste-and-recycling/waste-framework-directive_en) (accessed 2021 -05 -15).

641 (4) Gálvez-Martos, J.-L.; Styles, D.; Schoenberger, H.; Zeschmar-Lahl, B. Construction and  
642 Demolition Waste Best Management Practice in Europe. *Resources, Conservation and Recycling*  
643 **2018**, *136*, 166–178. <https://doi.org/10.1016/j.resconrec.2018.04.016>.

644 (5) Bridgwater, A. Fast Pyrolysis Processes for Biomass. *Renewable and Sustainable Energy*  
645 *Reviews* **2000**, *4* (1), 1–73. [https://doi.org/10.1016/S1364-0321\(99\)00007-6](https://doi.org/10.1016/S1364-0321(99)00007-6).

646 (6) Bridgwater, A. V. Review of Fast Pyrolysis of Biomass and Product Upgrading. *Biomass*  
647 *and Bioenergy* **2012**, *38*, 68–94. <https://doi.org/10.1016/j.biombioe.2011.01.048>.

648 (7) Mohan, D.; Pittman, C. U.; Steele, P. H. Pyrolysis of Wood/Biomass for Bio-Oil: A  
649 Critical Review. *Energy Fuels* **2006**, *20* (3), 848–889. <https://doi.org/10.1021/ef0502397>.

650 (8) Rahman, Md. M.; Liu, R.; Cai, J. Catalytic Fast Pyrolysis of Biomass over Zeolites for  
651 High Quality Bio-Oil – A Review. *Fuel Processing Technology* **2018**, *180*, 32–46.  
652 <https://doi.org/10.1016/j.fuproc.2018.08.002>.

653 (9) Yildiz, G.; Ronsse, F.; Duren, R. van; Prins, W. Challenges in the Design and Operation  
654 of Processes for Catalytic Fast Pyrolysis of Woody Biomass. *Renewable and Sustainable Energy*  
655 *Reviews* **2016**, *57*, 1596–1610. <https://doi.org/10.1016/j.rser.2015.12.202>.

- 656 (10) Margeriat, A.; Bouzegane, A.; Lorentz, C.; Laurenti, D.; Guilhaume, N.; Mirodatos, C.;  
657 Geantet, C.; Schuurman, Y. Catalytic Conversion of Beech Wood Pyrolytic Vapors. *Journal of*  
658 *Analytical and Applied Pyrolysis* **2018**, *130*, 149–158.  
659 <https://doi.org/10.1016/j.jaap.2018.01.015>.
- 660 (11) Bagnato, G.; Sanna, A.; Paone, E.; Catizzone, E. Recent Catalytic Advances in  
661 Hydrotreatment Processes of Pyrolysis Bio-Oil. *Catalysts* **2021**, *11* (2), 157.  
662 <https://doi.org/10.3390/catal11020157>.
- 663 (12) Kim, K. H.; Eom, I. Y.; Lee, S. M.; Choi, D.; Yeo, H.; Choi, I.-G.; Choi, J. W.  
664 Investigation of Physicochemical Properties of Biooils Produced from Yellow Poplar Wood  
665 (*Liriodendron Tulipifera*) at Various Temperatures and Residence Times. *Journal of Analytical*  
666 *and Applied Pyrolysis* **2011**, *92* (1), 2–9. <https://doi.org/10.1016/j.jaap.2011.04.002>.
- 667 (13) Wang, Z.; Burra, K. G.; Lei, T.; Gupta, A. K. Co-Pyrolysis of Waste Plastic and Solid  
668 Biomass for Synergistic Production of Biofuels and Chemicals-A Review. *Progress in Energy*  
669 *and Combustion Science* **2021**, *84*, 100899. <https://doi.org/10.1016/j.pecs.2020.100899>.
- 670 (14) Phakedi, D.; Ude, A. U.; Oladijo, P. O. Co-Pyrolysis of Polymer Waste and Carbon-  
671 Based Matter as an Alternative for Waste Management in the Developing World. *Journal of*  
672 *Analytical and Applied Pyrolysis* **2021**, *155*, 105077. <https://doi.org/10.1016/j.jaap.2021.105077>.
- 673 (15) Anuar Sharuddin, S. D.; Abnisa, F.; Wan Daud, W. M. A.; Aroua, M. K. A Review on  
674 Pyrolysis of Plastic Wastes. *Energy Conversion and Management* **2016**, *115*, 308–326.  
675 <https://doi.org/10.1016/j.enconman.2016.02.037>.
- 676 (16) Abnisa, F.; Wan Daud, W. M. A. A Review on Co-Pyrolysis of Biomass: An Optional  
677 Technique to Obtain a High-Grade Pyrolysis Oil. *Energy Conversion and Management* **2014**, *87*,  
678 71–85. <https://doi.org/10.1016/j.enconman.2014.07.007>.
- 679 (17) Wang, X.; Kersten, S. R. A.; Prins, W.; van Swaaij, W. P. M. Biomass Pyrolysis in a  
680 Fluidized Bed Reactor. Part 2: Experimental Validation of Model Results. *Industrial &*  
681 *Engineering Chemistry Research* **2005**, *44* (23), 8786–8795. <https://doi.org/10.1021/ie050486y>.
- 682 (18) Hwang, I.-H.; Kobayashi, J.; Kawamoto, K. Characterization of Products Obtained from  
683 Pyrolysis and Steam Gasification of Wood Waste, RDF, and RPF. *Waste Management* **2014**, *34*  
684 (2), 402–410. <https://doi.org/10.1016/j.wasman.2013.10.009>.
- 685 (19) Stoye, D.; Funke, W.; Hoppe, L.; Hasselkus, J.; Curtis, L. G.; Hoehne, K.; Zech, H.-J.;  
686 Heiling, P.; Yamabe, M.; Dören, K.; Schupp, H.; Küchenmeister, R.; Schmitthenner, M.;  
687 Kremer, W.; Wiczorrek, W.; Gempeler, H.; Schneider, W.; White, J. W.; Short, A. G.; Blank,  
688 W. J.; Calbo, L. J.; Plath, D.; Wagner, F.; Haller, W.; Rödder, K.-M.; Streitberger, H.-J.; Urbano,  
689 E.; Laible, R.; Meyer, B. D.; Bagda, E.; Waite, F. A.; Philips, M.; Köhler, K.; Simmendinger, P.;  
690 Roelle, W.; Scholz, W.; Valet, A.; Slongo, M.; Molz, T.; Hiller, R.; Thomer, K. W.; Vogel, K.;  
691 Schernau, U.; Hüser, B.; Brandt, A.; Milne, A.; Weyers, H.; Plehn, W.; Lentze, H.-A. Paints and  
692 Coatings. In *Ullmann's Encyclopedia of Industrial Chemistry*; Wiley Online Library, 2006.  
693 [https://doi.org/10.1002/14356007.a18\\_359.pub2](https://doi.org/10.1002/14356007.a18_359.pub2).

- 694 (20) Composition of paints [SubsTech]  
695 [https://www.substech.com/dokuwiki/doku.php?id=composition\\_of\\_paints](https://www.substech.com/dokuwiki/doku.php?id=composition_of_paints) (accessed 2021 -08 -  
696 12).
- 697 (21) Özbay, G.; ÖzçiFçi, A.; Kökten, E. S. The Pyrolysis Characteristics of Wood Waste  
698 Containing Different Types of Varnishes. *Turkish Journal of Agriculture and Forestry* **2016**, *40*  
699 (5), 705–714. <https://doi.org/10.3906/tar-1502-88>.
- 700 (22) Merk, V.; Chanana, M.; Gaan, S.; Burgert, I. Mineralization of Wood by Calcium  
701 Carbonate Insertion for Improved Flame Retardancy. *Holzforschung* **2016**, *70* (9), 867–876.  
702 <https://doi.org/10.1515/hf-2015-0228>.
- 703 (23) Merk, V.; Berg, J. K.; Krywka, C.; Burgert, I. Oriented Crystallization of Barium Sulfate  
704 Confined in Hierarchical Cellular Structures. *Crystal Growth & Design* **2017**, *17* (2), 677–684.  
705 <https://doi.org/10.1021/acs.cgd.6b01517>.
- 706 (24) Tan, H.; Ulusoy, H.; Peker, H. The Effects of Impregnation with Barite (BaSO<sub>4</sub>) on the  
707 Physical and Mechanical Properties of Wood Materials. *Journal of Bartın Faculty of Forestry*  
708 **2017**, *19* (2), 160–165. <https://doi.org/10.24011/barofd.346900>.
- 709 (25) Gan, D. K. W.; Chin, B. L. F.; Loy, A. C. M.; Yusup, S.; Acda, M. N.; Unrean, P.;  
710 Rianawati, E.; Jawad, Z. A.; Lee, R. J. An In-Situ Thermogravimetric Study of Pyrolysis of Rice  
711 Hull with Alkali Catalyst of CaCO<sub>3</sub>. *IOP Conference Series: Materials Science and Engineering*  
712 **2018**, *458*, 012085. <https://doi.org/10.1088/1757-899X/458/1/012085>.
- 713 (26) Lu, Q.; Zhang, Z.; Wang, X.; Dong, C.; Liu, Y. Catalytic Upgrading of Biomass Fast  
714 Pyrolysis Vapors Using Ordered Mesoporous ZrO<sub>2</sub>, TiO<sub>2</sub> and SiO<sub>2</sub>. *Energy Procedia* **2014**, *61*,  
715 1937–1941. <https://doi.org/10.1016/j.egypro.2014.12.247>.
- 716 (27) Sharifzadeh, M.; Sadeqzadeh, M.; Guo, M.; Borhani, T. N.; Murthy Konda, N. V. S. N.;  
717 Garcia, M. C.; Wang, L.; Hallett, J.; Shah, N. The Multi-Scale Challenges of Biomass Fast  
718 Pyrolysis and Bio-Oil Upgrading: Review of the State of Art and Future Research Directions.  
719 *Progress in Energy and Combustion Science* **2019**, *71*, 1–80.  
720 <https://doi.org/10.1016/j.pecs.2018.10.006>.
- 721 (28) Omais, B.; Courtiade, M.; Charon, N.; Thiébaud, D.; Quignard, A.; Hennion, M.-C.  
722 Investigating Comprehensive Two-Dimensional Gas Chromatography Conditions to Optimize  
723 the Separation of Oxygenated Compounds in a Direct Coal Liquefaction Middle Distillate.  
724 *Journal of Chromatography A* **2011**, *1218* (21), 3233–3240.  
725 <https://doi.org/10.1016/j.chroma.2010.12.049>.
- 726 (29) Chiantore, O.; Scalarone, D.; Learner, T. Characterization of Artists' Acrylic Emulsion  
727 Paints. *International Journal of Polymer Analysis and Characterization* **2003**, *8* (1), 67–82.  
728 <https://doi.org/10.1080/10236660304884>.
- 729 (30) Mikhailov, M. M.; Sokolovskiy, A. N.; Yuryev, S. A. Effect of Al<sub>2</sub>O<sub>3</sub> Nanoparticle  
730 Modification on Increase in Reflectivity of BaSO<sub>4</sub> Pigment. *Materials Chemistry and Physics*  
731 **2021**, *260*, 124099. <https://doi.org/10.1016/j.matchemphys.2020.124099>.

- 732 (31) Guan, L.; Fan, J.; Zhang, Y.; Guo, Y.; Duan, H.; Chen, Y.; Li, H.; Liu, H. Facile  
733 Preparation of Highly Cost-Effective BaSO<sub>4</sub>@BiVO<sub>4</sub> Core-Shell Structured Brilliant Yellow  
734 Pigment. *Dyes and Pigments* **2016**, *128*, 49–53. <https://doi.org/10.1016/j.dyepig.2016.01.013>.
- 735 (32) Hradil, D.; Grygar, T.; Hradilová, J.; Bezdička, P. Clay and Iron Oxide Pigments in the  
736 History of Painting. *Applied Clay Science* **2003**, *22* (5), 223–236. [https://doi.org/10.1016/S0169-1317\(03\)00076-0](https://doi.org/10.1016/S0169-1317(03)00076-0).
- 738 (33) Alvarez, V.; Williams, N. S. J.; Paulis, M. Isolation of the Interaction between CaCO<sub>3</sub>  
739 Filler and Acrylic Binder. Part I: Effect of the Surfactant and Functional Monomer Type.  
740 *Progress in Organic Coatings* **2019**, *136*, 105212.  
741 <https://doi.org/10.1016/j.porgcoat.2019.105212>.
- 742 (34) Channiwala, S. A.; Parikh, P. P. A Unified Correlation for Estimating HHV of Solid,  
743 Liquid and Gaseous Fuels. *Fuel* **2002**, *81* (8), 1051–1063. [https://doi.org/10.1016/S0016-2361\(01\)00131-4](https://doi.org/10.1016/S0016-2361(01)00131-4).
- 745 (35) Grønli, M. G.; Várhegyi, G.; Di Blasi, C. Thermogravimetric Analysis and  
746 Devolatilization Kinetics of Wood. *Industrial & Engineering Chemistry Research* **2002**, *41* (17),  
747 4201–4208. <https://doi.org/10.1021/ie0201157>.
- 748 (36) Roberts, A. F. A Review of Kinetics Data for the Pyrolysis of Wood and Related  
749 Substances. *Combustion and Flame* **1970**, *14* (2), 261–272. [https://doi.org/10.1016/S0010-2180\(70\)80037-2](https://doi.org/10.1016/S0010-2180(70)80037-2).
- 751 (37) Yang, H.; Yan, R.; Chen, H.; Zheng, C.; Lee, D. H.; Liang, D. T. In-Depth Investigation  
752 of Biomass Pyrolysis Based on Three Major Components: Hemicellulose, Cellulose and Lignin.  
753 *Energy Fuels* **2006**, *20* (1), 388–393. <https://doi.org/10.1021/ef0580117>.
- 754 (38) Palandri, A.; Gilot, P.; Prado, G. A Kinetic Study of the Decarbonation of CaCO<sub>3</sub>.  
755 *Journal of Analytical and Applied Pyrolysis* **1993**, *27* (2), 119–130.  
756 [https://doi.org/10.1016/0165-2370\(93\)80003-I](https://doi.org/10.1016/0165-2370(93)80003-I).
- 757 (39) Moya, R.; Gaitán-Álvarez, J.; Berrocal, A.; Araya, F. Effect of CaCO<sub>3</sub> on the Wood  
758 Properties of Tropical Hardwood Species from Fast-Growth Plantation in Costa Rica.  
759 *BioResources* *15* (3), 4802–4822. <https://doi.org/10.15376/biores.15.3.4802-4822>.
- 760 (40) Huang, L.; Yao, X.; Huang, Y.; Wang, Q. The Preparation of CaCO<sub>3</sub>/Wood Composites  
761 Using a Chemical Precipitation Method and Its Flame-Retardant and Mechanically Beneficial  
762 Properties. *BioResources* **2018**, *13* (3), 6694–6706. <https://doi.org/10.15376/biores.13.3.6694-6706>.
- 764 (41) Merk, V.; Chanana, M.; Keplinger, T.; Gaan, S.; Burgert, I. Hybrid Wood Materials with  
765 Improved Fire Retardance by Bio-Inspired Mineralisation on the Nano- and Submicron Level.  
766 *Green Chemistry* **2015**, *17* (3), 1423–1428. <https://doi.org/10.1039/C4GC01862A>.
- 767 (42) Pondelak, A.; Škapin, A. S.; Knez, N.; Knez, F.; Pazlar, T. Improving the Flame  
768 Retardancy of Wood Using an Eco-Friendly Mineralisation Process. *Green Chemistry* **2021**, *23*

769 (3), 1130–1135. <https://doi.org/10.1039/D0GC03852K>.

770 (43) Chen, S.; Chang, X.; Sun, G.; Zhang, T.; Xu, Y.; Wang, Y.; Pei, C.; Gong, J. Propane  
771 Dehydrogenation: Catalyst Development, New Chemistry, and Emerging Technologies.  
772 *Chemical Society Reviews* **2021**, *50* (5), 3315–3354. <https://doi.org/10.1039/D0CS00814A>.

773 (44) Li, C.-F.; Guo, X.; Shang, Q.-H.; Yan, X.; Ren, C.; Lang, W.-Z.; Guo, Y.-J. Defective  
774 TiO<sub>2</sub> for Propane Dehydrogenation. *Industrial & Engineering Chemistry Research* **2020**, *59* (10),  
775 4377–4387. <https://doi.org/10.1021/acs.iecr.9b06759>.

776 (45) Hoekstra, E.; Kersten, S. R. A.; Tudos, A.; Meier, D.; Hogendoorn, K. J. A. Possibilities  
777 and Pitfalls in Analyzing (Upgraded) Pyrolysis Oil by Size Exclusion Chromatography (SEC).  
778 *Journal of Analytical and Applied Pyrolysis* **2011**, *91* (1), 76–88.  
779 <https://doi.org/10.1016/j.jaap.2011.01.006>.

780 (46) Lu, Q.; Zhang, Z.; Yang, X.; Dong, C.; Zhu, X. Catalytic Fast Pyrolysis of Biomass  
781 Impregnated with K<sub>3</sub>PO<sub>4</sub> to Produce Phenolic Compounds: Analytical Py-GC/MS Study.  
782 *Journal of Analytical and Applied Pyrolysis* **2013**, *104*, 139–145.  
783 <https://doi.org/10.1016/j.jaap.2013.08.011>.

784 (47) Lin, X.; Kong, L.; Cai, H.; Zhang, Q.; Bi, D.; Yi, W. Effects of Alkali and Alkaline Earth  
785 Metals on the Co-Pyrolysis of Cellulose and High Density Polyethylene Using TGA and Py-  
786 GC/MS. *Fuel Processing Technology* **2019**, *191*, 71–78.  
787 <https://doi.org/10.1016/j.fuproc.2019.03.015>.

788 (48) Pattiya, A.; Titiloye, J. O.; Bridgwater, A. V. Fast Pyrolysis of Cassava Rhizome in the  
789 Presence of Catalysts. *Journal of Analytical and Applied Pyrolysis* **2008**, *81* (1), 72–79.  
790 <https://doi.org/10.1016/j.jaap.2007.09.002>.

791 (49) Staš, M.; Auersvald, M.; Kejla, L.; Vrtiška, D.; Kroufek, J.; Kubička, D. Quantitative  
792 Analysis of Pyrolysis Bio-Oils: A Review. *Trends in Analytical Chemistry* **2020**, *126*, 115857.  
793 <https://doi.org/10.1016/j.trac.2020.115857>.

794 (50) Hu, Y.; Li, J.; Wang, S.; Xu, L.; Barati, B.; Cao, B.; Wang, H.; Xie, K.; Wang, Q.  
795 Catalytic Fast Hydrolysis of Seaweed Biomass with Different Zeolite Catalysts to Produce  
796 High-Grade Bio-Oil. *Process Safety and Environmental Protection* **2021**, *146*, 69–76.  
797 <https://doi.org/10.1016/j.psep.2020.08.019>.

798 (51) Ennaert, T.; Van Aelst, J.; Dijkmans, J.; De Clercq, R.; Schutyser, W.; Dusselier, M.;  
799 Verboekend, D.; Sels, B. F. Potential and Challenges of Zeolite Chemistry in the Catalytic  
800 Conversion of Biomass. *Chemical Society Reviews* **2016**, *45* (3), 584–611.  
801 <https://doi.org/10.1039/C5CS00859J>.

802 (52) Palizdar, A.; Sadrameli, S. M. Catalytic Upgrading of Beech Wood Pyrolysis Oil over  
803 Iron- and Zinc-Promoted Hierarchical MFI Zeolites. *Fuel* **2020**, *264*, 116813.  
804 <https://doi.org/10.1016/j.fuel.2019.116813>.

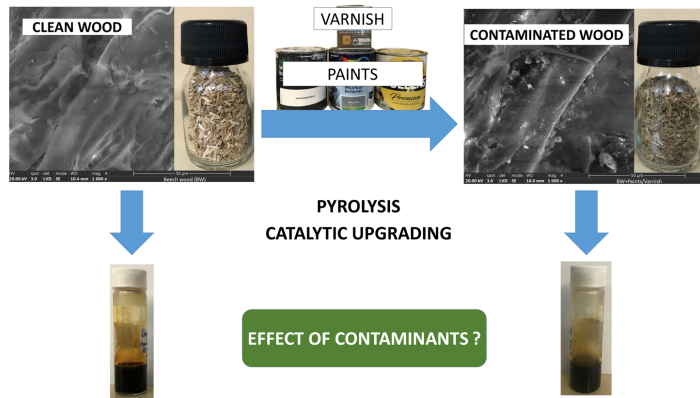
805

806

807

### TOC graphic

808



809